Schweizerische Eidgenossenschaft
Confédération suisse
Confederazione Svizzera
Confederaziun svizra

Federal Department of the Environment, Transport, Energy and Communications DETEC

Swiss Federal Office of Energy SFOE
Energy Research and Cleantech

Final Draft report 15 April 2020 (under review)

Slurry-HP II

Development of a super-cooling ice slurry heat pump system for solar heating applications

INSTITUT FÜR SOLARTECHNIK

Date: 15 April 2020

Location: Rapperswil

Publisher:
Swiss Federal Office of Energy SFOE
Energy Research and Cleantech
CH-3003 Bern
www.bfe.admin.ch

Subsidy recipients:
SPF Institute for Solar Technology, HSR University of Applied Sciences Rapperswil
Oberseestr. 10 CH-8640 Rapperswil

Authors:
Dr. Daniel Carbonell, Dani.Carbonell@spf.ch
Daniel Philippen, Daniel.Philippen@spf.ch
Dr. Mihaela Dudita, Mihaela.Dudita@spf.ch
Jeremias Schmidli, Jeremias.Schmidli@spf.ch
Maike Shubert, Maike.Shubert@spf.ch
Kevin Erb, Kevin.Erb@spf.ch
Stefan Brunold, Stefan.Brunold@spf.ch

SFOE project coordinators:
Carina Alles, carina.alles@bfe.admin.ch
Stephan Renz, renz.btr@swissonline.ch

SFOE contract number: SI/501641-01

The authors bear the entire responsibility for the content of this report and for the conclusions drawn therefrom.

Contents

Abstract

The Slurry-HP II project provided the first steps towards the development of a supercooling heat exchanger used as evaporator in heat pumps that can be utilized in solar ice-slurry heating applications. A solar ice-slurry system is a particular case of solar-ice system with the main difference that no heat exchangers are present in the ice storage when the slurry concept is applied. This is expected to reduce installation cost by approximately 10 %. Although our idea was originated to provide heating demands to residential buildings, the concept of supercooling ice slurry and the methods developed in this project can be applied for residential, commercial and industrial refrigeration, too.

Within the project we aimed to find the most promising available icephobic coatings developed for atmospheric conditions and assess them for supercooling applications. Thus, a key question for us was: *How will coatings developed for atmospheric conditions perform when immersed in water and submitted to forced convection?* To try to answer this question we developed a methodology to characterize icephobic coatings with the goal to select the best candidates to be used in future supercoolers. During the project another question arose: *Are state-of-the-art testing methods for atmospheric conditions enough and reliable to characterize coatings for immersed applications with a fluid in motion?* We should say that we could not clearly answer the second question within this project. Regarding the first one, we did some progress as explained below.

To assess the icephobic capabilities of the different coatings, experiments were conducted at two levels. Firstly, coated samples of 5 cm x 5 cm were evaluated at atmospheric conditions. Secondly, coated tubes of 1.5 m length and 6 cm outer diameter were used to assess the performance under immersed conditions with water flows. Experiments at sample level were used to select from a long list of 18 coatings, the three coatings finally applied to the tubes.

At sample level, the measurement that provided more information was the CAH which seemed to correlated well with results of tube experiments. However, the low number of tested tubes (only three) is not enough to confirm any correlation. Ice adhesion of most of the coated samples were well below of that of stainless steel (SS). The seven coating analysed in the ice adhesion test achieved between 3 to 23 times lower ice adhesion compared to SS. We could not observe a clear relationship between ice adhesion and receding CA or CAH.

Finally three coated tubes were compared to a reference polished SS tube (roughness of 0.2 μm) with water flows. Four water flow rates were used for the experiments, 400 kg/h, 800 kg/h, 1600 kg/h and 2000 kg/h corresponding to a range of water velocities on the freezing region of 0.09 m/s to 0.44 m/s. The lowest ice-free temperature at low mass flows (400 kg/h and 800 kg/h) was achieved by the coating based on a fluorochemical modified urethane (m2) with improvements of 40 % with respect to SS. The coatings based on an hybrid organic/inorganic sol-gel (d1) and silicon rubber (d2) had an improvement of 30 % and 25 % respectively. However, the coating m2 suffered from a clear degradation (coating was pilled off) after few weeks of testing and high mass flows (1600 kg/h and 2000 kg/h) could not be measured. This coating showed visual defects from the very beginning of the test. The other two coatings d1 and d2 did not show any visual defect. The best coating analysed at tube level was the d1 which performed best in overall and showed no degradation at all.

The improvement of coatings with respect to the SS should be taken with caution. The SS tube was experimentally evaluated for low mass flows at the beginning of the testing phase and these results were compared to the coated tube ones. Once all coated tubes were tested, and before testing the high mass flows of the SS, some improvements of the test setup were necessary. Afterwards, we conducted experiments at low mass flows for the SS again to see if results were similar to those obtained at the beginning. Surprisingly, results of the SS for low mass flows improved significantly from those obtained in the past. The reasons of such an improvement are not clear. We believe that the better fixing of the concentricity of the coaxial tube for the new SS and possible air in the system at the first experiments of SS might have an effect. For low mass flows the m2 had improvements of 11 % to 17 % compared to the new SS results. For high mass flows, where experiments of m2 were not possible due to degradation, d1 had 11 % higher performance at 1600 kg/h, but very similar at 2000 kg/h. Thus, these results leave us with a large uncertainty on the real improvements of the coatings analysed and a new set of experiments will be necessary. Fortunately, there is a running project (www.tri-hp.eu) where tube experiments are being conducted by the authors.

Zusammenfassung

Mit dem Projekt Slurry-HP II wurden die ersten Schritte zur Entwicklung eines Wärmetauschers zur Unterkühlung (supercooling) von Wasser unternommen. Der Wärmetauscher soll als Verdampfer in Wärmepumpen eingesetzt werden können und somit in solaren Eisbrei/Ice Slurry-Heizungsanwendungen. Eine solare Eisbrei-Heizung ist ein besonderer Fall einer Solar-Eis-Heizungsanwendung, da keine Wärmetauscher im Eisspeicher vorhanden sind. In einer Vorstudie wurde abgeschätzt, dass dies die Installationskosten um etwa 10 % reduziert. Obwohl unsere Idee ursprünglich zur Wärmeversorgung von Wohngebäuden entwickelt wurde, kann das Konzept auch für die Kühlung von Wohngebäuden, Gewerbe und Industrie verwendet werden.

Im Projekt wurde darauf abgezielt, eisabweisende Beschichtungen für atmosphärische Bedingungen zu finden und sie bezüglich ihrer Eignung zur Unterkühlung von fliessendem Wasser zu bewerten. Es stellte sich für uns deshalb folgende Frage: *Wie werden die für atmosphärische Bedingungen entwickelten Beschichtungen funktionieren, wenn sie in Wasser getaucht und erzwungener Konvektion ausgesetzt werden?* Um diese Frage möglichst beantworten zu können, entwickelten wir eine Methode zur Charakterisierung eisabweisender Beschichtungen mit dem Ziel, die besten Beschichtungen für den Einsatz in Wärmetauschern auszuwählen. Während des Projekts stellte sich eine weitere Frage: *Sind gängige Testmethoden für atmosphärische Bedingungen zuverlässig genug, um Beschichtungen zu charakterisieren, die von einer Flüssigkeit überströmt werden?* Diese zweite Frage konnte im Rahmen des Projekts nicht eindeutig beantwortet werden. Bei der Beantwortung der ersten Frage haben wir einige Fortschritte gemacht, wie im Folgenden erläutert wird.

Um die eisabweisenden Eigenschaften der ausgewählten Beschichtungen zu beurteilen, wurden Experimente in zwei Stufen durchgeführt. Zuerst wurden beschichtete Proben (Bleche von 5 cm x 5 cm) unter atmosphärischen Bedingungen untersucht. Anschliessend wurden beschichtete Rohre von 1,5 m Länge und 6 cm Aussendurchmesser verwendet, um die Unterkühlung bei Überströmung mit Wasser zu analysieren. Es wurden 18 Beschichtungen unter atmosphärischen Bedingungen getestet und drei beschichtete Rohre.

Bei der Analyse der 18 Proben konnte mit der Messung der Kontaktwinkelhysterese (CAH) die beste Korrelation zu den Ergebnissen der anschliessend durchgeführten Rohrexperimenten erreicht werden. Die geringe Anzahl der getesteten Rohre von lediglich drei reicht jedoch nicht aus, um diese Korrelation sicher bestätigen zu können. Bei den durchgeführten Zugversuchen lag die Eishaftung auf den meisten beschichteten Proben deutlich unter derjenigen von rostfreiem Stahl. Die sieben Beschichtungen, die im Eishaftungstest analysiert wurden, erzielten im Vergleich zu rostfreiem Stahl eine 3 bis 23 Mal geringere Eishaftung. Wir konnten keinen eindeutigen Zusammenhang zwischen Eishaftung und zurückweichendem Kontaktwinkel (CA) oder der Kontaktwinkelhysterese (CAH) feststellen.

Die Unterkühlung von Wasser wurde für drei beschichtete Rohre und ein Referenzrohr aus poliertem Edelstahl (Rauhigkeit von 0,2 μm) verglichen. Für die Experimente wurden vier Fliessgeschwindigkeiten verwendet, 400 kg/h, 800 kg/h, 1600 kg/h and 2000 kg/h. Niedrigste Temperaturen ohne Eisbildung auf dem Testrohr wurde bei geringen Massenströmen (400 kg/h and 800 kg/h) durch eine Beschichtung auf der Basis eines fluorochemisch modifizierten Urethans (Probe "m2") erreicht. Das Ergebnis mit dieser Beschichtung konnte dabei um 40 % gegenüber dem Edelstahlrohr verbessert werden. Die Beschichtungen auf der Basis eines hybriden organisch/anorganischen Sol-Gels (d1) und eines Silikonkautschuks (d2) zeigten eine Verbesserung von 30 % bzw. 25 %. Die Beschichtung m2 zeigte jedoch nach einigen Wochen deutliche Beschädigungen (Abplatzen), weswegen hohe Massenströme (1600 kg/h and 2000 kg/h) nicht gemessen werden konnten. Die beiden anderen Beschichtungen d1 und d2 wiesen keine visuell erkennbaren Mängel auf. Die Beschichtung d1 zeigte bei den Überströmversuchen insgesamt die besten Resultate und zeigte kein Ablösen von der Metalloberfläche des Rohrs.

Das bessere Abschneiden der Beschichtungen in Bezug auf die Referenz (Edelstahl) sollte jedoch mit Vorsicht behandelt werden. Die Referenz wurde zu Beginn der Tests mit geringen Massenströmen vermessen und diese Ergebnisse wurden mit denen der beschichteten Rohre verglichen. Nachdem alle beschichteten Rohre getestet waren und bevor die hohen Massenströme an der Referenz getestet wurden, waren einige Verbesserungen des Versuchsaufbaus notwendig. Danach führten wir erneut Experimente mit niedrigen Massenströmen für die Referenz durch, um zu sehen, ob die Ergebnisse ähnlich wie zu Beginn waren. Überraschenderweise

verbesserten sich die Ergebnisse der Referenz aber für niedrige Massenströme im Vergleich zu den in der Vergangenheit erzielten Ergebnissen signifikant. Die Gründe für eine solche Verbesserung sind nicht klar. Es ist möglich, dass nach Änderung des Versuchsaufbaus die idealerweise konzentrischen Rohre genauer ausgerichtet waren und dass Lufteinschlüsse im System bei den ersten Versuchen der Referenz die Messergebnisse beeinflussten. Für geringe Massenströme zeigte Beschichtung m2 im Vergleich zu den neuen Ergebnissen der Referenz Verbesserungen von lediglich 11 bis 17 %. Für hohe Massenströme, bei denen Experimente mit Probe m2 aufgrund von Degradation nicht möglich waren, hatte die Schicht d1 bei 1600 kg/h eine um 11 % niedriger Temperatur ohne Eisbildung, aber bei 2000 kg/h eine sehr ähnliche Temperatur. Es besteht also eine grosse Unsicherheit bei der Aussagekraft der durchgeführten Versuche mit überströmten Oberflächen und die Durchführung verbesserter Experimente scheint angezeigt. Erfreulicherweise können die Unterkühlungsversuche im Rahmen eines weiteren Projekts (www.tri-hp.eu) von den Autoren fortgesetzt werden.

List of Acronyms

ASHP	Air Source Heat Pump
CA	Static contact angle
CAH	Contact angle hysteresis
d1	Coating based on hybrid organic/inorganic sol-gel
d2	Coating based on silicon rubber
GSHP	Ground Source Heat Pump
m2	Coating based on fluorochemical modified urethanes
Ra	Surface roughness
SFH	Single Family Home
SS	Stainless Steel
IRF	Ice reduction factor

1 Introduction

For reaching the targets of the Swiss Energy Strategy 2050 it is necessary to raise the share of renewable energy in the building sector. One way is by combining different known technologies in new and proper ways. An example is the combination of solar thermal and heat pump systems with ice storages, the so-called solar-ice systems. The interest in solar-ice systems is growing with particular intensity in Switzerland. A likely explanation of the market push in Switzerland is related to regulations that restrict drilling of boreholes in some areas. Currently, solar-ice systems are installed when either air or ground source heat pumps are not wanted or not possible due to, for example, regulations for water protection or noise. For this reason, solar-ice systems have been established as an alternative to air/ground source heat pump systems. Due to the investment cost, medium to large residential buildings are the most common application.

Heat pumps can have several heat sources, such as air, ground or solar. There is not one single type of source for the heat pump that can cover the majority of heating demands in a cost-efficient way. Moreover, local regulations and social factors such as acceptance of relevant stakeholders can add barriers to some technologies. Thus, all heat sources are necessary to adapt to the large variety of technological, social and economic conditions existing in the building sector.

- **Air source heat pumps (ASHP)** are low cost and easy to install. However, their efficiency is limited, the social acceptance is sometimes low due to the noise emissions of the fan, aesthetics of external heat exchangers or space needs in the surroundings of the building.
- **Ground source heat pumps (GSHP)** have been used for heating and cooling for several decades and, normally, are very efficient. The main disadvantages of GSHP compared to ASHP are: the need for available ground to drill boreholes, possible conflicts with water/ground regulations, and higher investment cost.
- **Solar source heat pumps with ice storage (solar-ice)**. The term solar-ice is used for systems that combine solar thermal collectors with a heat pump and water as an intermediate storage medium that releases latent heat when being frozen by the heat pump in winter.

Solar-ice systems are direct competitors of GSHP systems with some advantages. They do not need ground space (if the ice storage is placed in the cellar), are not affected by ground water regulations, and can be very efficient in many climates where solar irradiation is high enough in winter. The high efficiency is reached

thanks to periods in which solar heat can provide useful heat directly, without using the heat pump, with efficiencies up to fifty times higher compared to a GSHP system (only circulation pumps of the solar circuit consume energy). Moreover, the ice storage can be at temperatures above ground level during most of the year, i.e. from May to November, and below when ice is present, e.g. from December to February (Carbonell et al., 2016c).

The solar ice-slurry system is a particular case of solar-ice systems. Both concepts are using solar thermal collectors as the heat source for the heat pump. Further, low temperature heat sources like waste water could be used as well. Regarding the type of solar collectors, mostly collectors with non-glazed absorbers are used. As long as the sun shines or the ambient temperature is not too low, solar collectors act as a direct source for the heat pump. During cold nights or days with low irradiation, when the low-grade energy from the solar collectors is insufficient to provide enough heat for the heat pump directly, the ice storage is used as a temporary heat source. The ice storage can store low-grade heat from solar collectors with a high volumetric storage capacity, increasing the solar energy yield by a factor of two compared to a solar system without an ice storage (Carbonell et al., 2016b).

In the solar ice-slurry system a typical brine to water heat pump is replaced by a water to water heat pump with a special evaporator called supercooler. A supercooler is a heat exchanger that is able to supercool water, e.g. from 0 °C to −2 °C without forming ice (Ernst and Kaufeld, 2016). At the outlet of the supercooler, water in liquid phase will be pumped to an ice slurry storage where nucleation will take place thanks to an ice-releaser or by direct contact with the ice particles from the storage. This innovation will eliminate the need for heat exchangers in the ice storage itself. This is expected to reduce the system installation cost by at least 10 %. Moreover, the heat exchanger (supercooler) is always free of ice and thus the heat pump is expected to have a higher efficiency, e.g. 15 % at 50 % ice fraction. To achieve this goal, an evaporator able to supercool water without producing ice needs to be developed.

The development of the slurry heat pump targeting heating applications does not exist yet. In order to be able to develop such a heat pump, several steps are necessary. The first one consist on finding and characterizing icephobic coatings that could be used for the supercoolers, which is the overall objective of the present project. These icephobic coatings are expected to increase the achievable supercooling degree without crystallisation in a heat exchanger compared to bare metals.

1.1 Motivation

One of the main barriers that solar-ice systems used for space heating and domestic hot water preparation are facing today is the installation cost. Usually today's cost are still higher compared to ground source heat pumps, which are able to achieve a similar energetic efficiency. Therefore, innovations to reduce the installation cost are needed for the deployment of solar-ice systems and thus for raising the share of solar energy in heating applications.

A relevant contribution to the solar-ice system's cost is related to heat exchangers. Several heat exchanger concepts are used today in ice storages for heating applications. Some examples of possible heat exchangers are shown in Fig. 1.1. The concepts shown in the upper part of Fig. 1.1 as well as on the bottom right picture, can be described as ice-on-hx, where hx stands for heat exchanger. Several heat exchangers such as e.g. coils, capillary mats and flat plates can be used. In ice-on-hx concepts, the whole ice storage volume needs to be filled with equally distributed heat exchangers. Another concept is shown in the bottom left picture of Fig. 1.1. This concept is currently entering the Swiss market and it is based on the thermal de-icing concept developed at SPF (Philippen et al., 2012).

In the thermal de-icing concept, the heat exchanger area can be reduced significantly compared to traditional ice-on-hx. Moreover, the heat exchanger surface is more frequently free of ice. However, the de-icing concept have some drawbacks such as the cost of the heat exchangers used, the complex control and hydraulics and the lower ice fraction allowed. Usually, the benefits of the de-icing concept are not enough to reduce the installation cost significantly compared to ice-on-coil concepts that make use of inexpensive plastic heat exchangers.

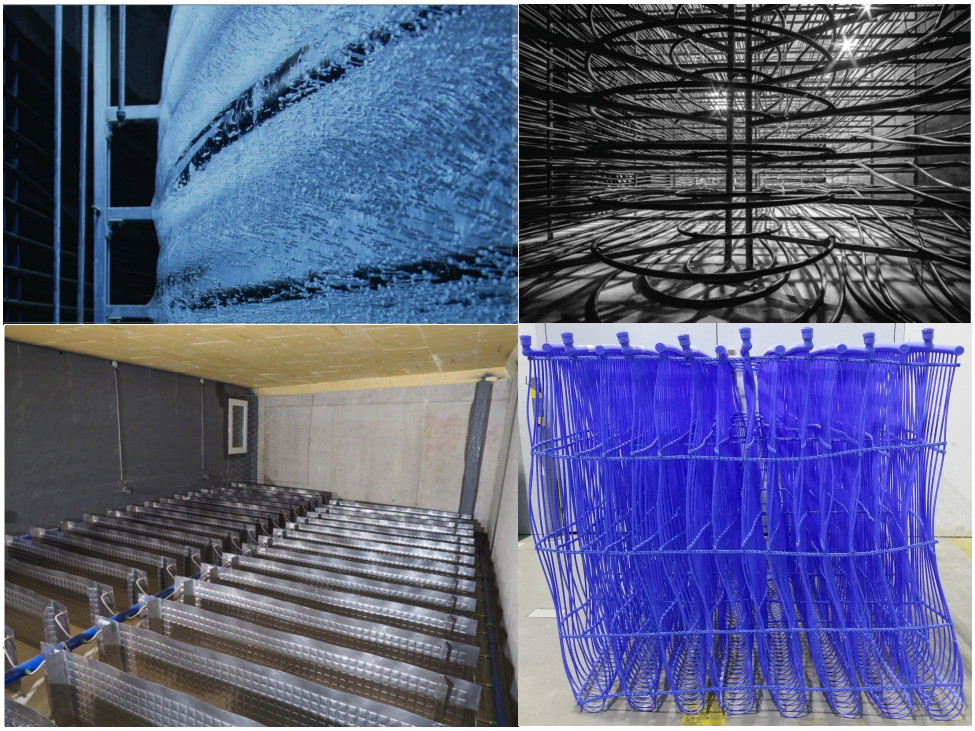

Figure 1.1: Top: Heat exchangers from Viessmann (`https://www.viessmann.ch`). Bottom left: heat exchangers from Energie Solaire in the SPF concept developed for EWJR (Philippen et al., 2014). Bottom right: capillary mats from CLINA tested in Carbonell et al. (2016a).

The idea behind Slurry-HP II is to avoid the use of any heat exchanger in the ice storage and thus to be able to reduce the installation cost significantly. Besides the cost reduction, the supercooling method could ensure an always free-of-ice condition on the surface of the heat exchanger. A feasibility study carried out in the previous project (Carbonell et al., 2017b) has shown that solar-ice systems based on the ice slurry supercooling approach have a high potential for cost reduction, while having a high energetic efficiency, especially for ice storage volumes of at least $1\,m^3$ per MWh of yearly heating demand, which corresponds well to ice storage volumes used today for multi-family buildings. The system efficiencies, investment and heat generation costs were compared to the best performing solar-ice configurations simulated as well as to current ground source heat pump systems. The cost distribution for the most promising solar-ice system simulated in Carbonell et al. (2017c) is shown in the left picture of Fig. 1.2 for a single-family house in Zurich. Details of cost assumptions can be found in Chapter 5 of Carbonell et al. (2017a). It can be seen that materials and installation of the ice storage heat exchangers accounts for 12 % of the reference solar-ice system cost. Eliminating this 12 % and considering an additional cost reduction on the storage casing since the support to keep the ice underwater is not required, would lead to a cost reduction of 13 %. The share of the heat pump in the complete system cost is 15 %. Thus, adding an estimated 6 % cost increase on the heat pump unit due to the supercooling heat exchanger, results in a reduction of the total investment cost of 11 %.

An example of the simulated system efficiencies and estimated heat generation cost for a single family house (SFH) in Zürich are shown in the right picture of Fig. 1.2 with the corresponding reference cost for a ground source heat pump. It can be observed that a solar ice-slurry system with $1.5\,m^2$/MWh of collector area and $1\,m^3$/MWh of ice storage volume per MWh of yearly heat demand, has a seasonal performance factor (SPF_{SHP+}) of 4.8 with lower heat generation cost compared to GSHP systems.

In summary, the feasibility study conducted previously (Carbonell et al., 2017b) lead to the conclusion that a slurry heat pump system based on the supercooling technology can be an attractive solution to reduce the cost of the system while improving the system efficiency. However, several technological challenges need to

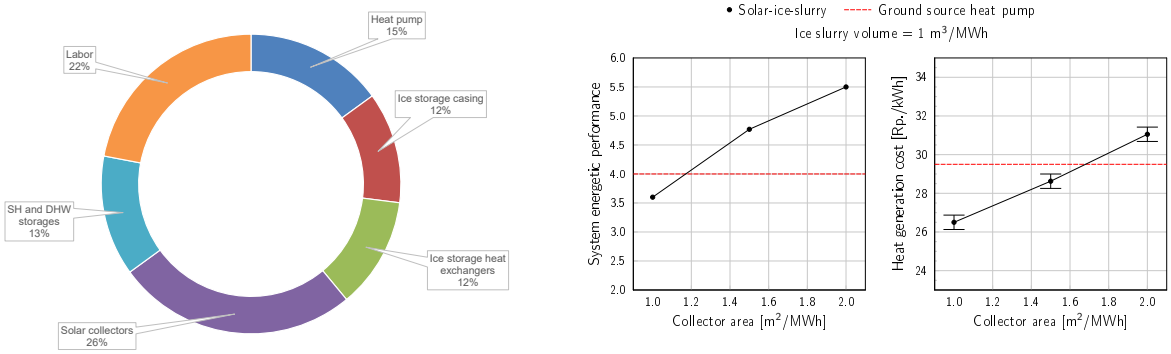

Figure 1.2: Left: installation cost shares for a state-of-the-art ice storage used in solar-ice systems (Carbonell et al., 2017a). Right: System seasonal (yearly) performance factor and heat generation cost for the potential ice-slurry system in comparison to state-of-the-art ground source heat pump system. Results obtained from Carbonell et al. (2017b).

be solved, i.e. to develop an evaporator able to supercool water in a reliable and stable way, the so-called supercooler. In this project we focus on the characterization and analysis of coatings that could be used for such a supercooler.

1.2 Objectives

An overall goal towards the development of a supercooling ice slurry heat pump system for solar heating applications is to proof the concept of heat exchangers operated with supercooled water. Since this goal is very ambitious and the technological risk are high, several intermediate steps are necessary. The Slurry-HP II projects aims to do the first steps toward the final goal. Specific objectives of the current project are:

1. Find the most promising currently available icephobic coatings that could delay ice formation.
2. Develop a methodology to characterize icephobic coatings for underwater applications.
3. Analyse the freezing point depression (degree of supercooling) and its stability as a function of coating, fluid velocity and temperature of the coated surface.

1.3 Icephobicity : current understanding

Icephobic is understood as a term that considers both delayed ice nucleation and low ice adhesion. This means that icephobic materials are not only expected to delay freezing of water, but when ice is formed, ice should have a weak adhesion, so that it could be easily removed. As icephobic materials are considered the hydrophobic materials, with low surface free energy, and superhydrophobic ones, which combine a low surface free energy with a nanotextured structure.

Most of the research found in the literature is focused on icephobic coatings for atmospheric conditions, i.e. used in the presence of air. Examples of applications include wind turbines, airplane wings, power transmission, telecommunications and marine applications to cite some. The ice nucleation and growth mechanism is different depending on the environment, operating conditions and on the pathway of ice-formation: from vapour to liquid and then solid, e.g. condensation of water droplets and freezing of condensed water in atmospheric conditions, or liquid to solid, e.g. freezing of supercooled water (Schutzius et al., 2015).

A limited number of studies is referring to underwater superhydrophobic coatings (Hejazi et al., 2013, Jones et al., 2015, Marmur, 2006, Xue et al., 2016, Zhang et al., 2015), where a typical application is to reduce fuel consumption caused by ice formation on ship hulls. Another field of interest is the reduction of marine

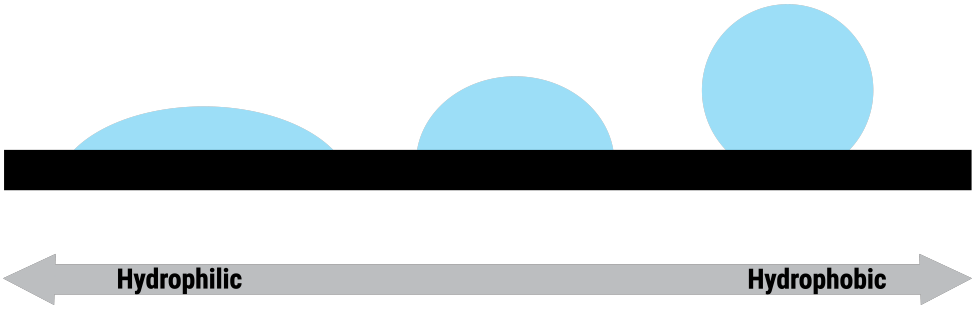

Figure 1.3: Surface wetting characteristics: hydrophilic and hydrophobic surfaces

bio-fouling, since some researchers found out that coatings that work as anti-fouling also show good icephobic properties (Upadhyay et al., 2017).

The most common practice when trying to design a coating is to completely avoid ice formation. However, coatings without imperfections do not exist and thus icing will be formed sooner or later, as these imperfections will serve as nucleation points. Thus, a second approach consist to control ice formation instead of completely avoiding it. Using the latter idea, Zwieg (2005) developed an ice repellent coating using also some hydrophilic points in order to ensure that ice starts to nucleate on specific locations where it can be easily removed by the water flow.

1.3.1 Relation between icephobicity and surface wetting

The current understanding of icephobicity and its relation with surface wetting is based on atmospheric conditions. Hejazi et al. (2013) defined the main desirable characteristics of icephobic materials. First, they should prevent or delay ice formation, and when ice is formed they should have a low ice adhesion. A value of 100 kPa was suggested, although this value is somewhat arbitrary (Nosonovsky and Hejazi, 2012). Considering the surface wettings properties, coatings can be defined as hydrophilic and hydrophobic (see Fig. 1.3). Surface properties, mainly surface wetting, expressed via contact angle (defined in section 2.1), and surface roughness, are correlating with icephobicity.

Rough hydrophilic surfaces are usually on a Wenzel state (see Fig. 1.4), therefore, a rough surface allows water to penetrate to cavities increasing the ice adhesion when the water freezes. On the other hand, hydrophobic surfaces are in the Cassie wetting state, with air pockets trapped between the solid ice and the water droplet. These air cavities become air voids when water freezes and serve as stress concentrators to break the ice. As long as the Cassie state is maintained, the contact surface is reduced and the ice adhesion is decreased. However, if the Cassie state is lost and water penetrates into the cavities, then the ice adhesion will increase significantly, since more area compared to a smooth surface is available between the ice and the substrate. This is the case for superhydrophobic surfaces, which are typically rough and have low contact angle hysteresis (defined in section 2.1) thanks to the Cassie state. However, the Cassie state will evolve irreversibly to a Wenzel state with increased CA hysteresis (Stone, 2012). Once the substrate is fully wetted, superhydrophobic surfaces show higher ice adhesion compared to a smooth surface and an increasing amount of energy is required to remove the ice (Kim et al., 2012).

Different studies regarding icephobic coatings were based on the idea that superhydrophobic materials were good candidates to repeal water, thus they would be also good candidates for icephobic coatings. It was thought that ensuring a non wetting of the surface (indicated by high contact angles) would allow to avoid ice formation. Today, there is evidence (Hejazi et al., 2013, Jung et al., 2011, Kulinich et al., 2011, Nosonovsky and Hejazi, 2012, Sojoudi et al., 2016) that this is not always true and thus, it can be concluded that superhydrophobic materials are not necessarily icephobic.

Nosonovsky and Hejazi (2012) suggested that ice adhesion, measured as the force needed to separate ice from

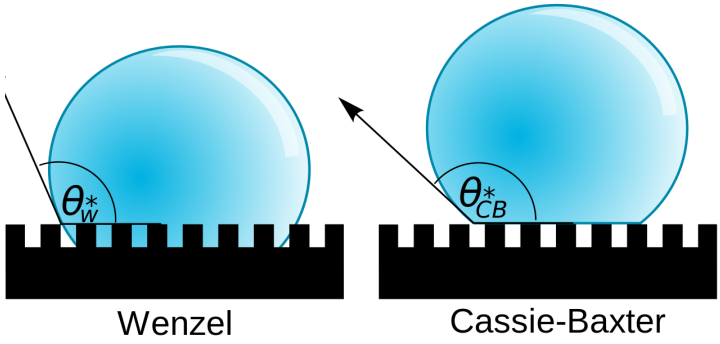

Figure 1.4: Wetting models for superhydrophobic surfaces: (left) homogenous wetting (Wenzel), the liquid follows the solid surface and penetrates into the roughness grooves, (right) heterogeneous wetting (Cassie) where air or another fluid is trapped underneath the liquid, inside the roughness grooves and the liquid is in contact only with top asperities. Picture from `https://de.wikipedia.org/wiki/Datei:Contact_angle_microstates.svg`

the substrate, was a function of the receding contact angle (CA, defined in section 2.1). It was argued that the energy related to separate two surfaces depends on the receding CA, and the energy involved in bringing them together with the advancing CA. However, it was concluded that although icephobicity (expressed as low ice adhesion) correlates with high receding CA, the size of the microcracks at the solid-ice interface is a critical parameter that governs ice adhesion. Thus, some superhydrophobic surfaces can have strong ice adhesion if the voids at the interface are not large enough.

Hejazi et al. (2013) measured experimentally the ice adhesion on several samples and the following conclusions were drawn: i) ice adhesion was not related to CA or receding CA, but to the CA hysteresis (CAH); ii) the relation with surface roughness was not clear; iii) the bouncing-off effect of incoming droplets was similar in superhydrophobic and icephobic surfaces.

The relation between ice adhesion and contact angle hysteresis was also observed by Janjua et al. (2017). Ice adhesion was negligible for CAH below 25°. The maximum ice adhesion was in the range of 170 kPa, corresponding to a CAH of around 90°. The ice adhesion decreased for values below but also above the CAH of 90°. The degradation of all coated samples, i.e. the increase of the CAH, was significant after 10 to 20 cycles of icing/deicing.

Kulinich and Farzaneh (2009) compared different superhydrophobic surfaces with high CA (from 140° to 153°) and different CAH, ranging from 5° to 90°. They found no correlation between CA and ice adhesion, but between CAH and ice adhesion. This was attributed to the higher solid-ice contact area on surfaces with high CAH. Superhydrophobic surfaces with CAH above 60° showed high ice adhesion, comparable to mirror polished aluminium (362 $\pm$ 26 kPa). Superhydrophobic materials with low CAH below 20° showed an ice adhesion below 100 kPa. Surfaces with low CAH and low ice adhesion had a higher roughness. Larger ice adhesion was found on samples with low roughness. It was argued that rough and more spiky surfaces had very small water-solid contact area and had lower ice adhesion. It was also observed that the ice formation rate on the sample was two times faster in samples with high CAH compared to samples with low CAH.

Kulinich et al. (2011) analysed different superhydrophobic coatings by spraying water microdroplets at temperatures below 0 °C. Ice adhesion was tested on several hydrophobic surfaces with different surface topographies and chemistry. The ice adhesion in a first test was in the range of 40 kPa to 80 kPa, well below the ice adhesion of a mirror polished aluminium ($\sim$360 kPa) and that of a flat fluoropolymer surface ($\sim$ 190 kPa). However, only after 20 cycles of icing-deicing, the ice adhesion increased to $\sim$ 200 kPa. When water freezes above the air trapped in the cavities, some asperities of the surface got indented into the ice. When ice was removed, these asperities were partially damaged. The gradual mechanical damage of the rough surface is expected to lead to larger water-solid contact. As a result, the CAH increases and the water repellency is deteriorated. Experiments under humid conditions lead to the conclusion that *wet* samples are not hydrophobic anymore. The CA decreased from 150° to 130° during 90 minutes of condensation and the ice adhesion increased from

$\sim$ 40 kPa to $\sim$ 130 kPa. Concluding, Kulinich et al. (2011) raised doubts about the use of superhydrophobic materials for anti-icing applications and they stated that even if one could develop a mechanically durable topography, the poor performance under humid air conditions seems to be difficult to overcome.

Farhadi et al. (2011) tested four nanotextured superhydrophobic samples and observed a large degradation of the ice repellency after 12 cycles of icing/deicing. The increase of ice adhesion was believed to be associated with the larger ice-solid contact area of the nanotextured surfaces after several icing/de-icing cycles. The coating deterioration was explained by the surface roughness decreasing, which correlated very well with the increase of ice adhesion on the tested samples. The decrease of roughness was explained by the sharp tips breaking, which were believed to be indented into the ice. Another possible reason provided was that the ice formation could induce interfacial stress damaging the coating. The effect of surface asperities that remain indented into ice, thus damaging the coating was also discussed by Ensikat et al. (2009). Farhadi et al. (2011) concluded by raising doubts about the use of nano-structuring and by proposing surfaces made of very rigid or elastic materials, which could show a good durability, thought these were not tested at that time yet.

Jung et al. (2011) analyzed experimentally freezing delays on surfaces ranging from hydrophilic to hydrophobic. It was observed that smooth surfaces with nanometer-scale roughness and higher wettability had freezing time delays one order of magnitude higher than superhydrophobic surfaces with larger roughness and low wettability. The highest ice delay was obtained for a hydrophilic untreated silicon wafer and two hydrophilic ultrananocrystaline diamond coatings. All these coatings had a very low roughness (1.4 nm to 6 nm). A significant freezing delay was achieved for samples with roughness comparable or smaller than the critical ice nucleus radius. Surfaces with similar roughness showed different freezing delays, which was mainly attributed to the different surface energy. It was concluded that while hydrophobic materials have higher resistance to ice formation than rough hydrophilic surfaces, very smooth hydrophilic surfaces, i.e. with roughness very close to the critical nucleus radius, showed better icephobicity.

1.3.2 Icephobic coatings for underwater application

There is a very limited number of studies regarding the topic of icephobic coatings for underwater applications and most of them are focused on wetting/non-wetting phenomena, rather than on the ice effect under water. Moreover, all the studies cited below are based on water without forced movement, which is not the case we are targeting.

A theoretical feasibility study from Marmur (2006) indicated that maintaining a dry surface of superhydrophobic coatings immersed in water is, in principle, feasible and may be thermodynamically stable. These could be used as icephobic coatings for underwater applications if their surface could be maintained dry under water. A dry surface means that the ice formation as well as the ice adhesion are hindered. However, as far as we know, dry surfaces under water have not been proof for surfaces submitted to flows conditions.

Superhydrophobicity is usually achieved by tailoring the surface roughness and by enhancing the non-wetting properties via the trapped air pockets from roughness valleys. Keeping these surfaces dry under water is very challenging because trapped air can diffuse into the liquid (Jones et al., 2015). To maintain the air in these valleys, it is necessary to achieve a chemical equilibrium with the dissolved air in the surrounding liquid. If the liquid is supersaturated with air, an air layer covering the surface may be achieved indefinitely. However, if the liquid is undersaturated, the air within the pore will dissolve into the liquid.

Based on a theoretical analysis, Jones et al. (2015) predicted that surfaces could stay dry under water, even after trapped air has fully depleted, due to the stabilization of the vapor phase from the roughness valleys. It was assumed that roughness spacing of hundreds of nanometers or less, and not microns or larger, could achieve this target.

1.3.3 Lubricating layer as anti-icing design

Recent efforts for developing icephobic surfaces are based on decreasing the CAH, which can be achieved either by texturing the surface to decrease the contact area between water droplets and the substrate or by using an ultra smooth surface with low wettability, particularly in high humid conditions. However, any synthetic textured solid will have some defects arising from mechanical damage, which increases in time. These inhomogeneties can contribute to liquid pinning, freezing and ice adhesion. Wong et al. (2011) developed a radically different ice-repellent surface based on slippery, liquid-infused porous surfaces (SLIPS). The main assumptions of the SLIPS concept are that a liquid interface is intrinsically smooth and defect free down to molecular scale and provides self-repair by flowing due to capillary action to the damaged part of the substrate. The SLIPS concept, inspired by Nepenthes pitcher plants, uses a porous, nano/micro-structured substrate to retain the infused liquid. The liquid strongly forms a stable, defect-free and slippery interface. It was shown that these properties are insensitive to the precise geometry of the substrate, allowing to use inexpensive, low-surface-energy structured materials.

The design of SLIPS as ice repellent are based on three criteria:

- the lubricating liquid must preferentialy wet the substrate and be retained into the substrate. This is achieved by using micro/nano-textured rough substrates whose large surface area and the chemical affinity for the liquid facilitates complete wetting and adhesion of the lubricating fluid.
- the affinity between the fluid and the substrate should be higher than that of water and the substrate. This is achieved by defining the chemical and physical requirements between the substrate and the lubricating fluid.
- the lubricating fluid should be immiscible in water.

Kim et al. (2012) developed the concept of SLIPS as ice repellent using aluminium substrate. The CAH decreased from 41° to 2° from the untreated aluminium to the SLIPS. The ice adhesion strength decreased from 1350 kPa to 15.5 kPa, which was attributed to the ultra-smooth solid-liquid interface. It was found that lubricating aluminium samples that lack either surface roughness or proper surface chemistry did not noticeable improve the my droplet sliding behaviour because the substrate was not able to retain the lubricating fluid.

Chen et al. (2017) proposed a different approach than the SLIPS, but also using a liquid layer between the substrate and water. The main difference is that they propose to add chemical groups to a surface that create an aqueous lubricating layer that reduces ice adhesion. A self-sustainable lubricating layer (SSLL) was achieved by modifying the solid surface with highly water absorbing, hydrophilic poly(acrylic acid) (PAA). The strong association of water molecules with the PAA chain lead to an overlayer of hydration water that remained liquid-like down lo low temperatures. This concept is durable as long as water is present. The idea is based on the assumption that water exist in two states within a hydrophilic polymer. The liquid-like state is associated with the hydrophilic groups along the polymer chain to the extend that the well oriented hydrogen bonding is in locally favorable configuration to prevent this water from freezing. The remaining water can be frozen.

1.4 Summary of icephobicity

Icephobic coatings are based on materials with a low surface energy such as those based on polysiloxanes and fluoropolymers. To the best of our knowledge, there are no studies regarding the ice effect under circulating water, but rather on atmospheric conditions and few on water without forced convection. Superhydrophobic surfaces can prevent ice formation, but they are not necessarily icephobic as the water repellency and ice adhesion mechanisms are not the same (Hejazi et al., 2013, Jung et al., 2012, Nosonovsky and Hejazi, 2012). Moreover, with cycles of icing/deicing, the nanotextured surface is degrading leading to an increased ice adhesion (Kulinich et al., 2011, Kulinich and Farzaneh, 2009). Instead, smooth surfaces with roughness in the nanometer range show a tendency to prolong the freezing delay phenomenon and have better durability in comparison to nanotextured superhydrophobic surfaces with a similar chemistry (Jung et al., 2011). Thus, smooth hydrophobic surfaces, rather than rough superhydrophobic surfaces, seem to be better candidates for

retarding ice formation on long term in a supercooler. Method that introduce a lubricating layer between the substrate and the water might be promising. However, the key question is whether these coatings are stable when immersed in water and submitted to forced convection. Would it be possible to maintain the lubricating layer attached to the substrate for long periods? Is is possible to have a self-reparing layer?. Some authors have addressed this issue (Solomon et al., 2014, Wexler et al., 2015a,b) and it seems that technical problems are not solved yet. Moreover, these concepts are not yet ready to be applied to coat tubes in the meters scale we are aiming for.

2 Methodology

2.1 Key Performance Indicators (KPIs)

Considering the boundary conditions of SlurryHPII project and based on the literature review, the following Key Performance Indicators were defined in order to select the best icephobic coating:

Material related KPIs:

- Hydrophobic or superhydrophobic surface with high static contact angle (>90°)
- Low contact angle hysteresis (CAH<20°)
- Low ice adhesion (<100 kPa)

Durability related KPIs:

- Durability in static (no flow) conditions - no material modifications after at least 100 cycles of icing/de-icing cycles
- Durability in dynamic conditions: no visible degradation after three measurements campaigns

Dynamic test related KPIs:

- Coldest stable coated surface temperature on immersed tubes submitted to forced convection.

Contact angle: The performance of icephobic coatings strongly depends on the surface wetting characteristics (Fig. 1.3), as they are influencing the ice adhesion. The surface wetting is described by the contact angle (noted with θ, also called static contact angle) formed when a drop of a liquid (e.g. water) is placed on a solid (Fig. 2.1). This angle is determined by the properties of the solid and the liquid and it is an indication of how well the liquid will spread over a surface. When θ >90°, the surface is called hydrophobic, while for $\theta >$ 120° the term superhydrophobic is used. The smaller the contact angle, the weaker are the cohesive forces (between similar molecules, e.g. water molecules) compared with adhesive forces (between different molecules such as between water and solid molecules). In this case, molecules of the liquid tend to interact more with solid molecules then with liquid molecules. The larger the contact angle is, the stronger are the cohesive forces compared to adhesive forces and the molecules of the liquid tend to interact more with each other then with the solid molecules. Most icephobic surfaces are characterized by a high contact angle θ (shown in Fig. 1.3, right).

The contact angle can be defined by the Young equation (Eq. 1), where γ_w is the water surface free energy, γ_s is the solid surface free energy and γ_w, s is the solid/water interfacial free energy.

$$\gamma_s = \gamma_{w,s} + \gamma_w \cdot cos(\theta) \tag{1}$$

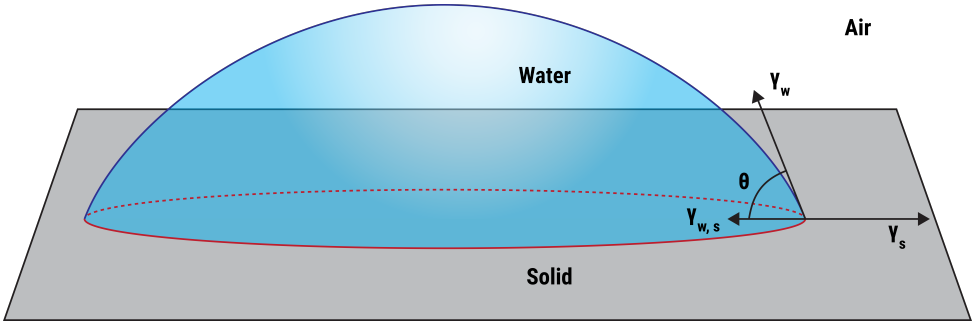

Figure 2.1: Contact angle formed by sessile liquid drop on a smooth homogeneous solid surface

In case of rough surfaces, wetting/non-wetting of rough surfaces is described by the apparent contact angle (noted with θ^*) and by the Wenzel, Cassie and Baxter equations (Eral et al. (2013)). The Wenzel equation (Eq. 2) is applied when all capillaries within a rough surface are filled with liquid and there is no air layer between surface and drop. This is also called *Wenzel state*. Wenzel state is common on surfaces with lower roughness or for a superhydrophobic surface in a supersaturated environment where condensed water can replace the air from the rough texture (Jung et al., 2012). The following notations are used in (Eq. 2): θ^* is the measured (apparent) contact angle, θ is the contact angle with the smooth surface and r' is the roughness coefficient (ratio between the overall surface and the apparent one - the surface projected geometrically onto a plane). This equation shows that in case of hydrophilic surfaces, the contact angle is smaller on a rough surface of the same material, while for hydrophobic surfaces, the contact angle is larger on a rough surface.

$$cos(\theta^*) = r'cos(\theta) \tag{2}$$

Cassie and Baxter have formulated another relationship for the situation in which only parts of the overall surface are in contact with the liquid (Cassie-Baxter wetting) Law and Zhao (2016). This is shown schematically in Fig. 1.4 and it is the case of the icephobic coatings with trapped air. According to these models, increased roughness will decrease the contact angle on hydrophilic surfaces, but increase the contact angle on hydrophobic surfaces. Thus, roughness amplifies both hydrophilicity and hydrophobicity (not necessarily linearly). The mechanisms governing wetting of rough surfaces are not yet fully understood.

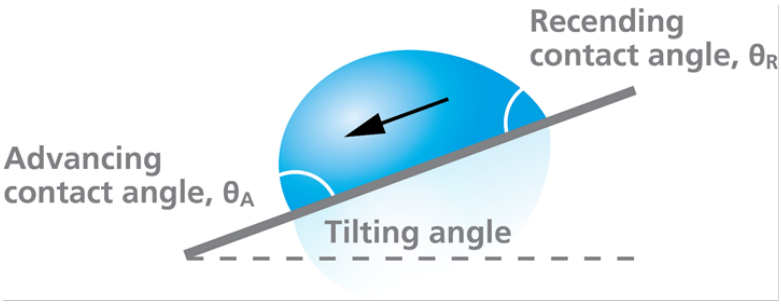

Figure 2.2: Scheme showing the advancing and receding contact angle using the tilted method (Source: Biolin Scientific)

In practice, an optical contact angle measuring device is used and the static contact angle is calculated by applying a tangent line from the contact point along the liquid-vapour interface in the droplet profile (Fig. 2.1).

Contact angle hysteresis: The contact angle hysteresis is calculated as the difference between the advancing and receding contact angle. There are several methods to measure the advancing and receding angles:

- *Needle method*: by varying the volume of the drop, used especially for superhydrophobic samples.
- *Wilhelmy method*: based on the force measurement, recommended for samples like thin fibers.
- *Tilting method*: the sample is tilted until the droplet starts to move. This method allows sample mapping.

In the current project, the tilting method was used for measuring the advancing and receding contact angles (schematically shown in Fig. 2.2), and thus for CAH calculation.

Ice adhesion: An essential KPI related to the performance of icephobic coatings is the ice growth and ice detachment quantified through the adhesion test. Imagine a drop of frozen water on top of a solid substrate. The ice adhesion is related to the work needed to remove the ice, meaning to break the bonds between ice and solid in the absence of deformations. This is called the thermodynamic work of adhesion and it is defined by Eq. 3, where $\gamma_{w,s}$ represent here the interfacial force between ice and the solid (Makkonen (2012)).

$$W_a = \gamma_s + \gamma_{ice} - \gamma_{ice,s} \tag{3}$$

Using the Young equation (Eq. 1), the work of adhesion W_a can be correlated with water contact angle as:

$$W_a = \gamma_{ice} + \gamma_w \cdot cos(\theta) + \gamma_{w,s} - \gamma_{ice,s} \tag{4}$$

Considering that the surface energies of water and ice are approximately the same and assuming that their interfacial energies at the solid interface are as well approximately the same, Eq. 4 can be simplified as:

$$W_a \simeq \gamma_w(1 + cos(\theta)) \tag{5}$$

Considering that the thermodynamic work of adhesion shows the ice adhesion strength, the equation Eq. 4 can be used to show the correlation between ice adhesion strength and water contact angle. In the present work, the ice adhesion strength was measured experimentally at HSR.

Currently, there is no standard methodology to measure the ice adhesion (Makkonen (2012)). This means that absolute values between different testing methods are difficult to compare. For this reason, the ice reduction factor (IRF), which relates the ice adhesion to a reference ice adhesion material, can be used. In our case, the stainless steel (SS) substrate was used as a reference. Of course this method is only useful if the same reference material is used between different studies. The IRF is defined as:

$$IRF = \frac{W_{a,ss}}{W_{a,coating}} \tag{6}$$

Coldest surface coating temperature The most relevant KPI to characterize the coatings when applied to a heat exchanger would be the supercooling degree, i.e. the difference between the water temperature at the outlet of the tube and the water freezing point (0 °C). However, the tubes experimentally used are not long enough to achieve high supercooling degrees and therefore other KPIs were necessary. Longer tubes were not possible for practical reasons such as too large oven size for curing the coatings. A possible KPI would be to monitor the brine temperature that would correspond to the coldest point of the water flow, i.e. at the tube tip. Two sensors were placed at that position (see sensor 2 and 3 in Fig. 2.12) to be able to monitor this temperature. However, this temperature does not consider the influence of the thickness of the coating and of the mass flow of the water. Thus, a more appropriate KPI would be the surface temperature at the coldest point of the water loop. However, a surface temperature sensor will act as a nucleating agent and therefore cannot be used to characterize the coatings. For this reason, a calculation of the surface temperature is necessary. In order to have reliable surface temperature results, experiments were conducted with the reference polished stainless steel tube with the surface temperature sensor added. This experiments were used to calibrate a model that allowed us to calculate the surface temperature as shown in section 4.2.

2.2 Testing methodology

The characterization of icephobic coatings was done in two steps. The first screening was based on experiments on coated samples of 25 cm^2 under atmospheric conditions and a second test was done using coated tubes with an outer diameter of 6 cm and a length of 1.5 m in immersed conditions submitted to forced convection.

2.2.1 Small samples under atmospheric conditions

The goal of testing small sample was to screen among available icephobic coatings and select the best performing coatings for the tube level tests.

For this, flat samples of 5 cm x 5 cm were tested in two steps. First, the surface properties and coatings durability were assessed. This was done by measuring the static contact angle and by performing cycles of icing/melting in a climatic chamber. After these investigations, only one coating had shown visible durability issues. Thus, a second method was used to try to distinguish between the remaining samples. The second approach consists of following measurements:

- Static contact angle.
- Advancing and receding contact angle and calculation of the contact angle hysteresis (CAH).
- Ice adhesion.

2.2.2 Immersed tubes with forced convection

Custom-made stainless steel tubes of 6 cm outer diameter and 1.5 m length were coated after polishing and cleaning with organic solvents. Then, the tubes were tested under immersed conditions with forced convection and a counterflow configuration (see experimental setup in Fig. 2.12).

Selected coatings from the first screening phase were used for these tube experiments. The experimental set-up consists of a coaxial tube where the brine circulates inside the tube. On the outside part of the tube, the coating was applied. Water flows in the annulus in a counterflow arrangement, between the coated tube and a transparent pipe, which allows visual observation of the coated surface. Temperature sensors were placed into the brine and the water. The surface temperature of the coldest point of the coated tube on the water side was calculated using the brine temperature, the water temperature at the outlet, and the heat transfer coefficients involved. As a reference, one polished stainless steel tube was used. The following testing procedure was applied for each tube:

- The brine temperature was decreased until 0 °C was achieved on the wall surface at the coldest point on the water side. The minimum mass flow possible for the set-up was used.
- The brine temperature was lowered by 0.2 K in the set-point of the chiller. These conditions were stabilized to ensure a stable operation. Including the cooling period, each step lasted two hours.
- The brine temperature was decreased step-wise using 0.2 K steps until freezing with step lengths of 2 hours.
- The same experiment was repeated several times in order to assess reproducible results (considering the stochastic nature of freezing).
- The same experiment was conducted using different mass flows in order to evaluate the effect of the flow velocity on the freezing temperatures. Four mass flows were evaluated, 400 kg/h, 800 kg/h, 1600 kg/h and 2000 kg/h.
- The coatings were characterized by the minimum temperature on the wall surface needed to produce freezing.

These experiments were conducted with the aim of selecting the best coatings for future heat exchangers.

2.3 Description of experimental set-ups for small samples tests

2.3.1 Set-up for contact angle and contact angle hysteresis

During the project, two types of optical contact angle measuring devices were used:

- Small, Mobile Surface Analyser (MSA - KRÜSS GmbH) from the IWK Institute for Materials Technology and Plastics Processing from HSR University of Applied Sciences Rapperswil.
- An OCA 35 Optical Contact Angle Meter (DataPhysics Instruments) from ETH's Laboratory of Thermodynamics in Emerging Technologies. The measurements were done using an OCA 35 Optical Contact Angle Meter (DataPhysics Instruments, Serial No: O35E0615F97A) with a tilting base unit (Fig. 2.3).

Contact angle at IWK-HSR The contact angle (Fig. 2.3) was measured using a Mobile Surface Analyzer. All samples were dried with purified air before the CA measurements. Five measurements of the contact angle for each sample were conducted to evaluate the surface uniformity and also for uncertainty assessment. The maximum, minimum and averaged CA were recorded.

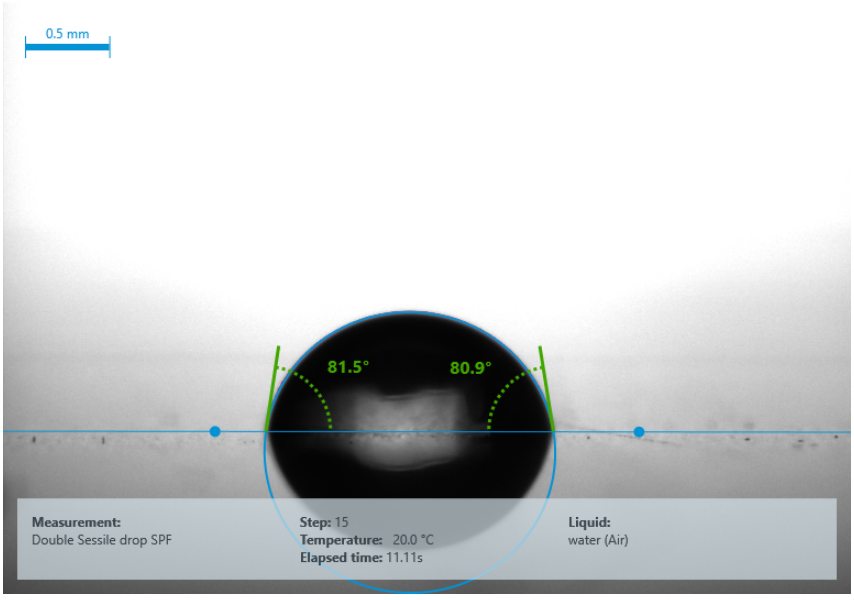

Figure 2.3: Example of the static contact angle determined using the KRÜSS Mobile Surface Analyzer from HSR-IWK and the sessile drop method.

Contact angle hysteresis (CAH) at ETH Both static and dynamic contact angles (advancing and receding angle, contact angle hysteresis) were measured at ETH's Laboratory of Thermodynamics in Emerging Technologies. A Hamilton glass syringe (1000 µL) was used to place water droplets (sessile drop method) with a dosing rate of 1 µL/s. The static contact angle was measured when the tilting base unit was horizontal (0°). For the measurement of dynamic contact angles (advancing, receding and hysteresis), the base unit was inclined slowly (relative velocity 1.02 °/sec) from its horizontal position to 50°. The device has the possibility to tilt the entire system and, in this way, the position of the sessile drop within the optical axis does not change. A droplet was placed on the sample and the same drop volume (20 µL) was used to compare the samples. Seven measurements were made for each sample and the average value was reported.

Surface Morphology The surface morphology was assessed using a simple scanning electron microscope available at the institute of IWK at HSR.

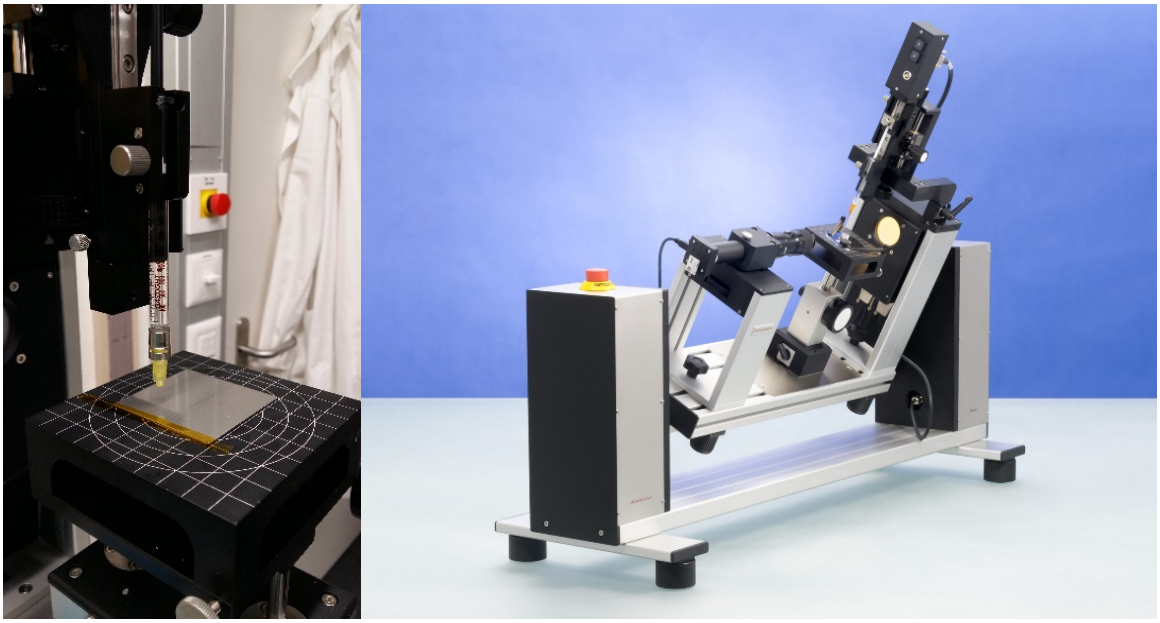

Figure 2.4: Setup for static contact angle measurements at ETH using the OCA 35 Optical Contact Angle Meter. Image showing the tilting base unit used to measure the contact angle hysteresis with the tilting method (Source: ETH, DataPhysics Instruments).

2.3.2 Set-up for icing/melting cycles

For evaluating the durability in static conditions, samples were immersed in water, iced and melted 230 times, using a climatic chamber (Horstmann HS 220 K 45, volume 0.22 m^3) from SPF (Fig. 2.5, left). A preliminary test was performed using a cooled sample holder for controlling the sample temperature (Lauda RK8 KP) (Fig. 2.5, right). Large water droplets were placed in the middle of the samples. The degradation was assessed using the contact angle. The contact angle was measured before and after the cycling with the MSA (mobile surface analyser) device. All samples were dried before the CA measurements.

2.3.3 Set-up for ice adhesion test

First approach with pulling force perpendicular to the sample. For the first ice adhesion test, cylindrical ice was formed on the coated samples and a force perpendicular to the surface was applied to remove the ice. The coated samples (50 x 50 mm plates) were placed in a sample holder made of aluminium alloy. An air gap between the sample and the sample holder was filled with water when preparing the samples for the test. A strong adhesion of the sample plate at the lower part of the sample holder was achieved by wetting the lower part with water that "glued" the sample onto the holder after freezing the water. The surface of the sample holder that was in contact with the ice on the coating was significantly smaller than the 50 mm $\times$ 50 mm of the sample to ensure that adhesion forces on the side of the coating are lower than the adhesion forces that stick the back side of the sample (not coated) to the sample holder.

Two diameters for the ice were tested: 40 mm (12.6 cm^2) and 20 mm (3.1 cm^2), with an ice thickness of 1.5 mm and 5 mm respectively. All relevant surfaces of the sample holder and the surface of the stainless steel (reference) samples were cleaned with alcohol before preparing the set-up. The surface of the coated samples were flushed with de-ionized water for cleaning.

The ice was formed using the climatic chamber. Different freezing profiles were tried out to analyse the

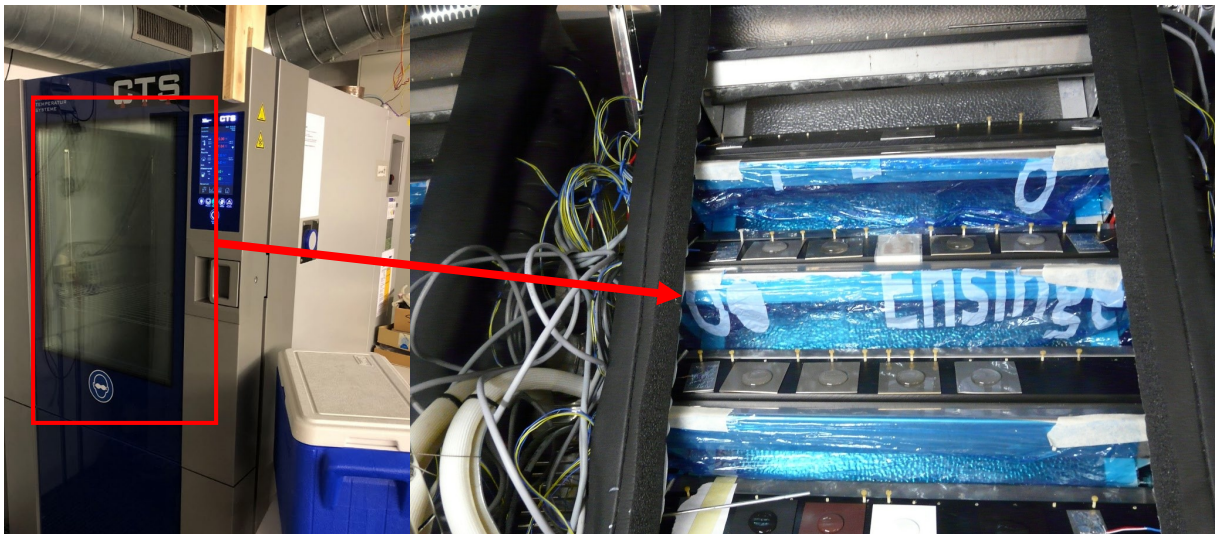

Figure 2.5: Left: climatic chamber to freeze the samples. Right: sample holder used for icing/de-icing experiments showing the samples and water droplets on different blocks of the sample holder .

influence on the ice cohesion force: a) −5 °C for 24 h; b) −30 °C for 18 h then 4 h warming to −4 °C; and c) −30 °C for 2 h then 18 h warming to −3.5 °C. The following water types were used in the different tests: tap water, ultra-pure water non-degassed (oxygen concentration: 10 mg/L) and degassed (1.2 mg/L).

The tests were done in a tensile test machine shown on the left of Fig. 2.6 (Shimadzu, Load cell SPL-10KNA). This machine has an integrated climatic chamber (see right picture from Fig. 2.6), that was kept at −4 °C during the ice adhesion tests. Each prepared sample was moved to the climatic chamber of the tensile machine using a mobile freezer.

Second approach with share stress test set-up. In order to measure the shear stress force on an iced surface it was necessary to construct another sample holder that could be used not only to freeze water on top of a coated sample as done in the method explained above, but it was also necessary to adapt this sample holder to the tensile machine in a way that the vertical pulling force of the tensile machine could be used to measure a shear stress. An scheme of this sample holder is shown in Fig. 2.7. The set-up described in this section was develop in the framework of a Master thesis (Rehm, 2019).

The main elements necessary to prepare the samples such as coated samples, sample holders and the pipette to add the water are shown in Fig. 2.8. Water is injected in the holes shown in the left picture of Fig. 2.7 and a layer of water with controlled thickness is formed on top of the coating. The thickness is given by the distance between the aluminium block and the structure (D) shown in Fig. 2.8. Eight aluminium blocks were made and used as sample holders. The aluminium surface from the sample holder in contact with water has been scratched in order to increase the ice adhesion and make sure that ice will be removed at the coating level first.

To freeze water, the same climatic chamber from the icing/melting experiments (see left picture of Fig. 2.5) was used. The support with a total of eight sample holders filled with water was cooled down to −20 °C and kept at this temperature level for 24 hours. No supercooling was present and a clear ice layer was formed. A surface sensor was placed on the aluminum block to monitor the temperature of the block. After the freezing

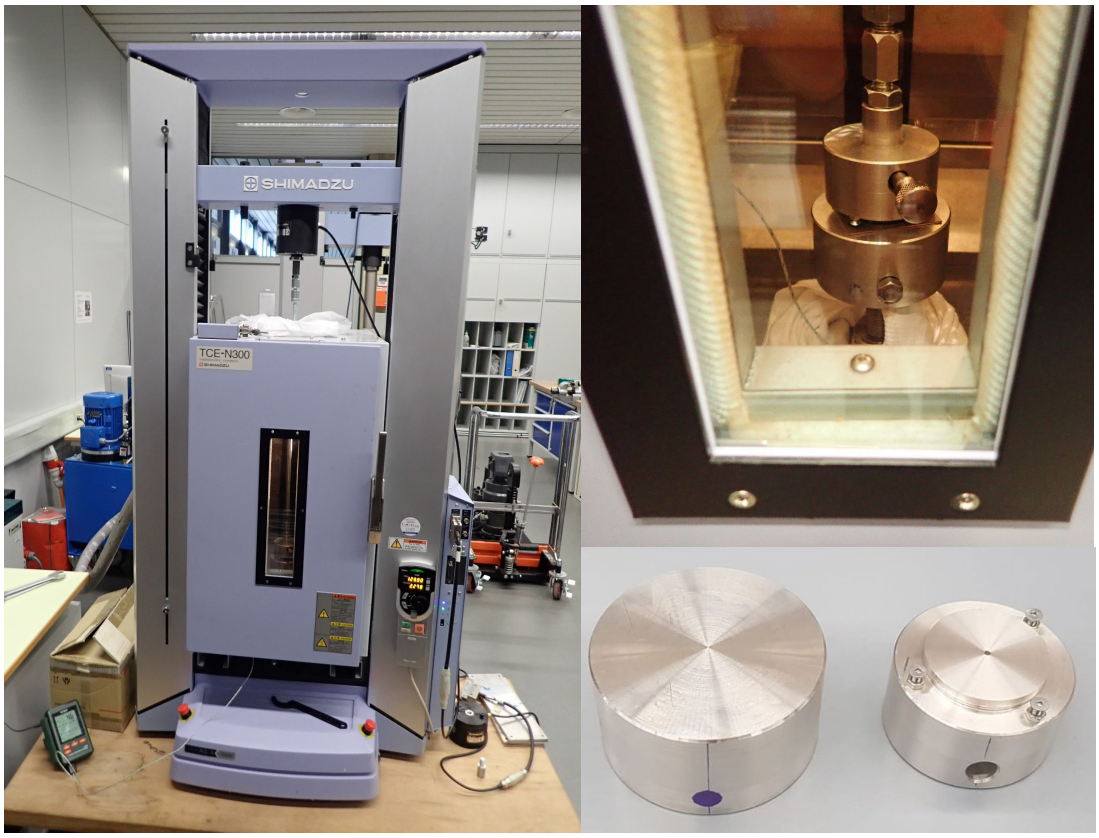

Figure 2.6: Left: tensile test machine with integrated climatic chamber used for the ice adhesion tests. Right (up) Ice adhesion test with force perpendicular to the sample surface: view into the climatic chamber with the sample holder (two large aluminium cylinders) which contains a coated sample plate and an ice layer that adheres to the coating and the upper part of the sample holder. Right (bottom) sample holder.

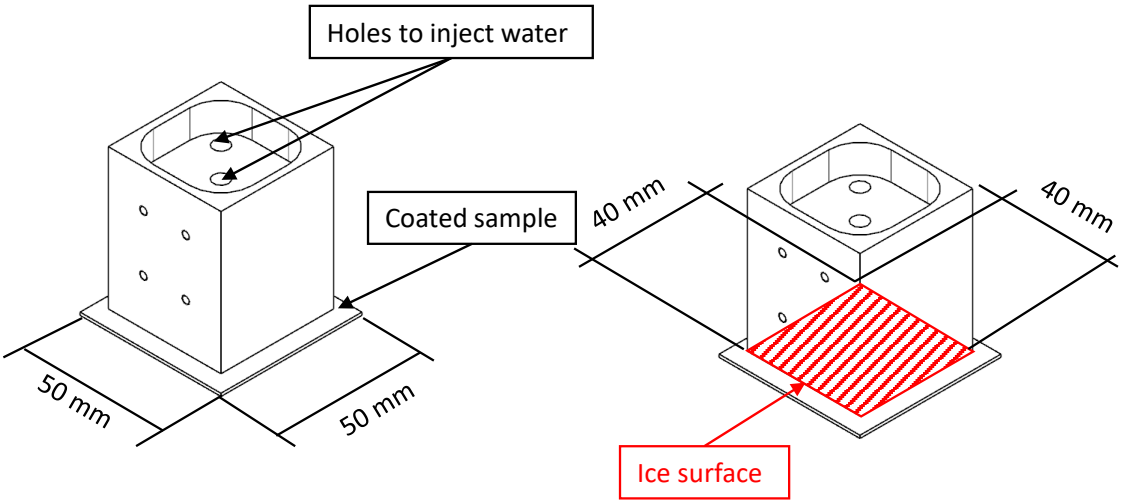

Figure 2.7: First prototype of Aluminium sample holder constructed for the second approach using shear stress. The last prototype had five holes to inject water with the same dimensions.

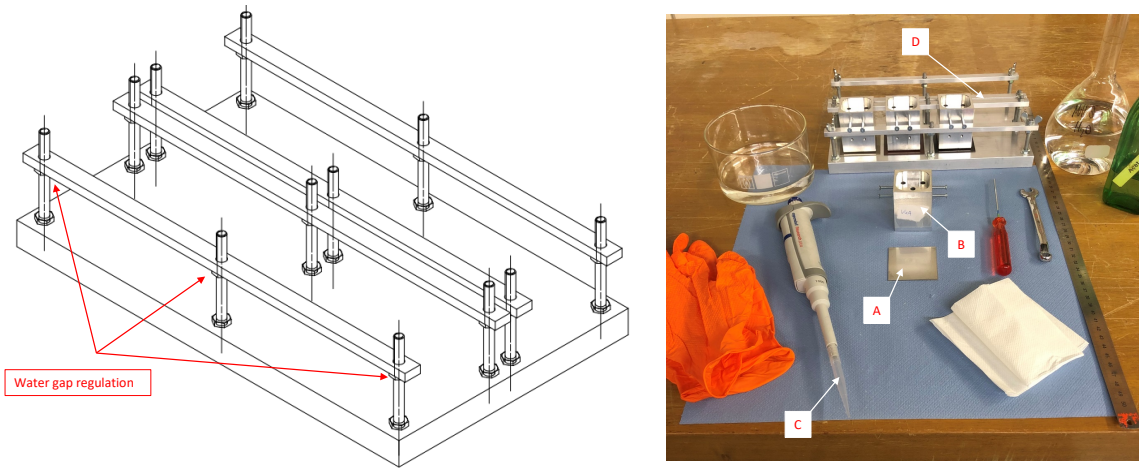

Figure 2.8: Left: Construction to fix eight sample holders (marked as D on the right picture) with the possibility to regulate the gap between the Aluminium surface and the coated sample. Right: different material used for the ice adhesion test. A: coated sample; B: sample holder; C: pipette used to add water droplets with controlled volume; D: construction (shown on the left picture) to allocate the sample holders and freeze them in the chiller together.

phase, the samples were kept at $-4\,^{\circ}\mathrm{C}$ and transported in a cold box to the tensile machine shown in Fig. 2.9. The sample holder was fixed in a small enclosure shown on the right picture of Fig. 2.9 and kept during the test at $-4\,^{\circ}\mathrm{C}$ using liquid nitrogen. Using the device shown in Fig. 2.10, a vertical force was applied. When this force is higher than the ice adhesion between the ice and the coated sample, then the sample holder will slide down and the ice adhesion strength expressed via the shear stress will be measured.

2.4 Laboratory setup for testing immersed coated tubes with forced convection

2.4.1 Preparation of stainless steel tubes

To manufacture the tubes for a immersed test with forced convection, a stainless steel tube was welded with a cone and a sealing cap so that the tube was closed at one side. The ensemble of the cone and the cap will be called hereafter as tip. This custom-made tip has a roundish end designed to smooth the flow and avoid possible turbulence that may cause nucleation. Shortly before the welded cone, a baffle plate was welded into the tube so that the glycol that circulates inside the tube cannot reach the tip. This plate ensures that the coldest point on the tube is before the tip and also before the welded part.

In order to obtain the required surface roughness of one micrometer necessary to apply the coatings with confidence, the welded seam as well as the entire tube were polished.

A setup was built to test the different coated tubes in flow condition, the schematic of the setup can be seen in Figure 2.12.

The internal part of the tube is connected to a Julabo FL11006 chiller, which uses a 50 % glycol/water mixture to cool down the tube from the inside. On the outside of the coated tube, water flows through an ABS and a PMMA tube in the opposite direction of the glycol, thus creating a counterflow coaxial arrangement. After the heat exchanger, the water flows into a storage. The water is pumped out of the tank, through a heater to remove possible ice particles being pumped from the storage, a flow measurement device, a water filter, and then it goes back into the heat exchanger. All components are insulated, to reduce heat gains into the system. A picture of the setup, as well as of the tip of the sample tube can be seen in Figure 2.13.

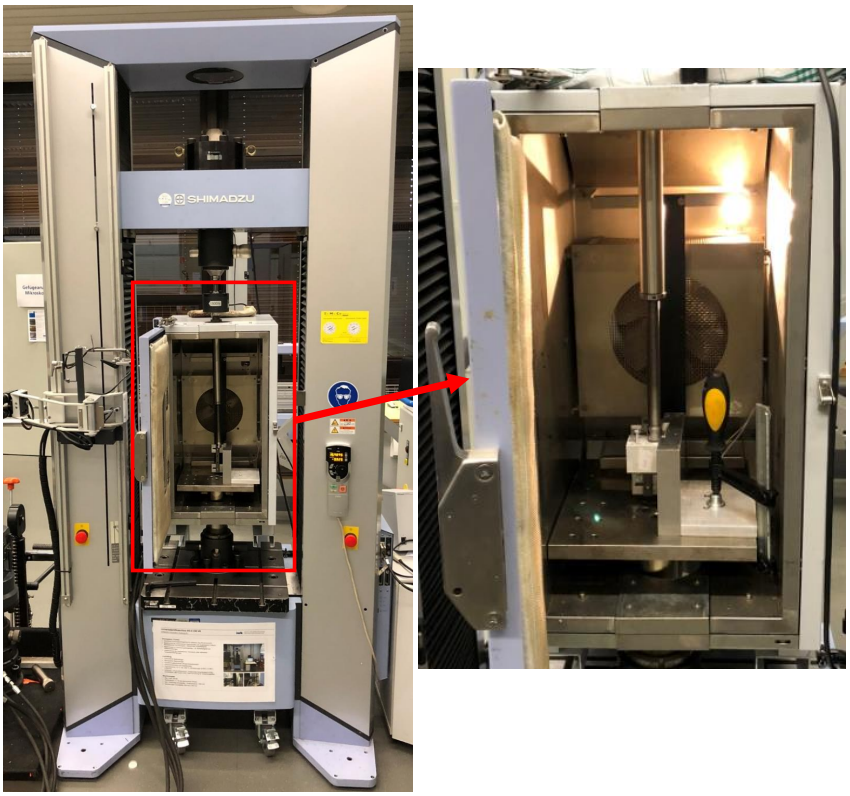

Figure 2.9: Left: Experimental set-up used for measuring the shear stress. Right: enclosure with controlled temperature used for ice adhesion test.

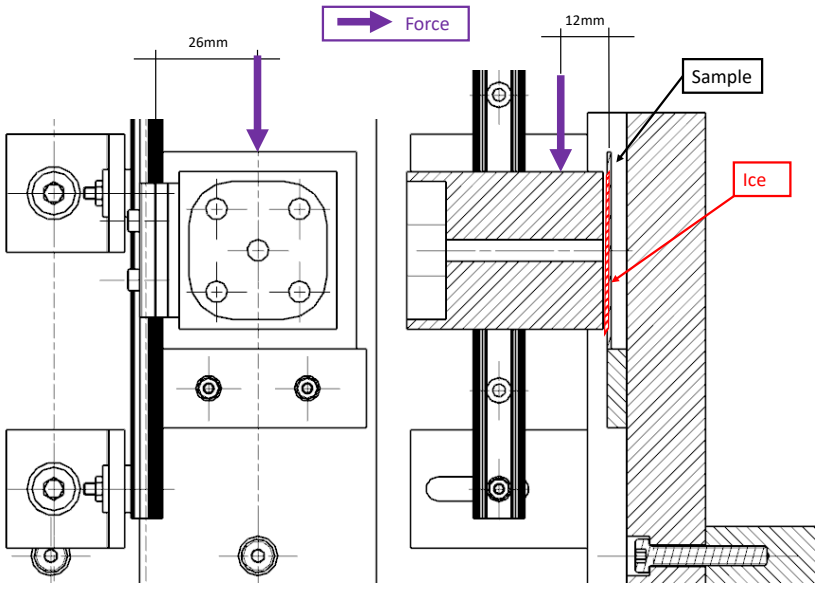

Figure 2.10: Front and side view of the sample holder and the component used for the ice adhesion using the shear stress method.

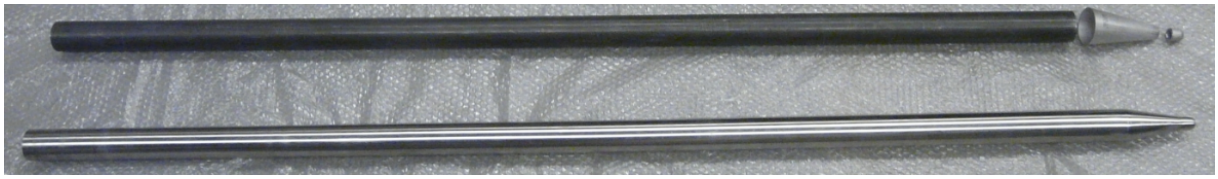

Figure 2.11: Parts needed to built the stainless steel tube and the tube after being sanded.

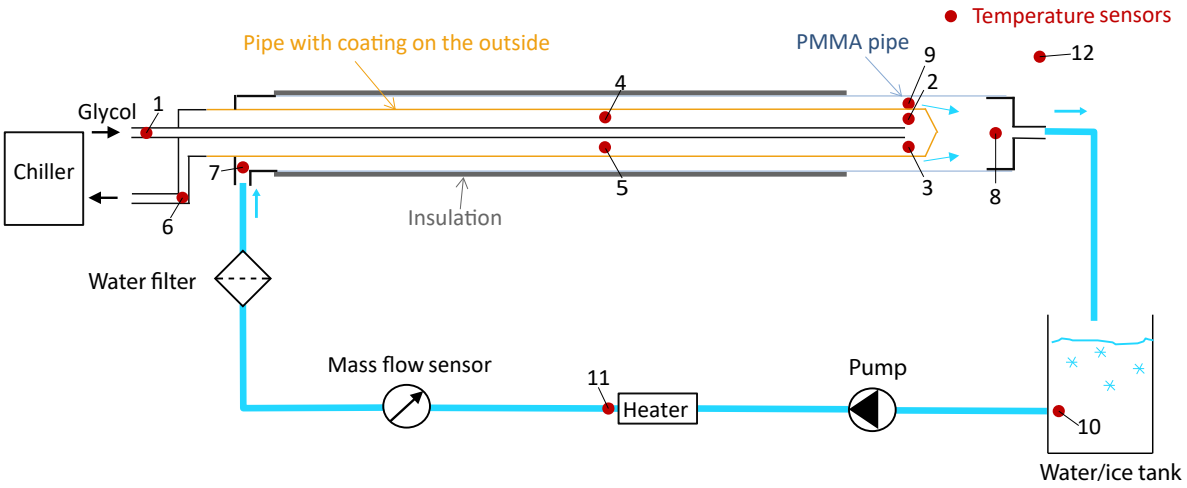

Figure 2.12: Schematic of the experimental setup used to test coated tubes under flow conditions.

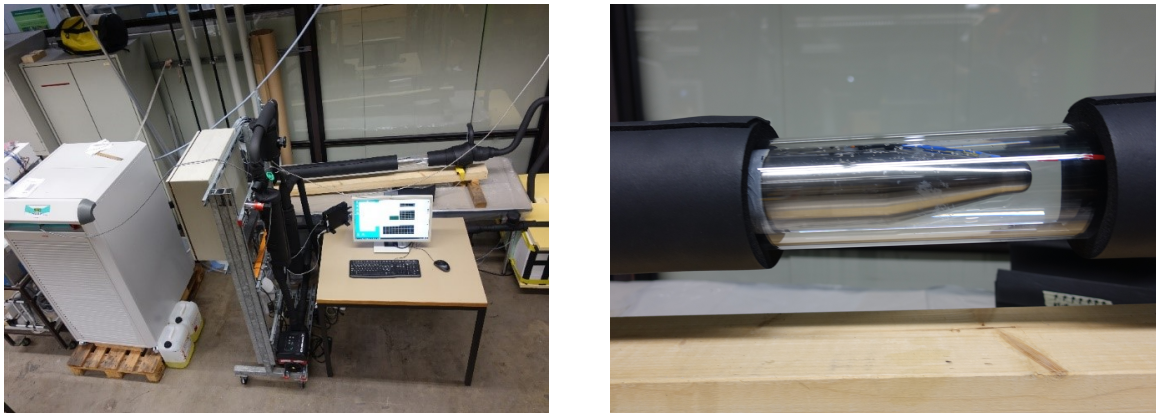

Figure 2.13: Left: Laboratory setup to test the coated tubes under flow conditions; right: tip of sample tube

Twelve temperature sensors were installed and calibrated. All temperature sensors and their specifications are listed in Table 2.1. The sensors in the water were calibrated using an ice-water mixture. The sensors in the brine loop were calibrated using a calibrator.

Table 2.1: Temperature sensors in experimental setup to test coated pipes

Sensor Number	Medium	Location	Calibration	Points	Accuracy in range of interest
			°C	°C	K
1	Glycol	Hx-Inlet	-10 to 0	0, -10	± 0.03
2	Glycol	Tip of coated tube	-10 to 0	0, -10	±0.03
3	Glycol	Tip of coated tube	-10 to 0	0, -10	±0.03
4	Glycol	Middle of coated tube	-10 to 0	0, -10	±0.03
5	Glycol	Middle of coated tube	-10 to 0	0, -10	±0.03
6	Glycol	Hx-Outlet	-10 to 0	0, -10	±0.03
7	Water	Hx-Inlet	-2 to 2	0	±0.03
8	Water	Hx-Outlet1	-2 to 2	0	±0.03
9	Water	Hx-Surface	-2 to 2	0	±0.03
10	Water	Storage	-2 to 2	0	±0.03
11	Water	Heater	-2 to 2	0	±0.03
12	Air	Ambient	15-30	n/a	±0.2

2.4.2 Automatic ice detection

The ice detection is determined using two different indicators. On the one hand, the pump power was used and, on the other hand, the temperature difference along the water loop. Both ice detecting methods have a start delay of 20 minutes at each new cycle. After the ice is detected, the coaxial tube is heated up to 20 °C for 40 minutes. The ice detection using the pump power is based on the pump power measurement. An average value of the last 10 minutes is calculated and compared with the actual value; if the actual value is greater than the average value plus 20 %, then icing is assumed. When ice is formed, the pressure lost of the system increases and the pump power will increase to maintain the target mass flow. The ice detection using the temperature difference method is based on the fact that ice formation will release the latent heat and the temperature will raise to 0 °C. An average value of the temperature difference over the water loop of the last 10 minutes is calculated continuously. If the actual value divided by the average value is less than 0.6 (60 %), then icing is assumed.

Calculation of water temperature at the surface: The supercooling degree can be assessed depending on the coldest point from the water cycle. The lowest water temperature is expected before the tip at the position that correspond to sensors 2 and 3 of Fig. 2.12. The surface temperature was measured for calibration purposes with a surface sensor placed on the stainless steel tube in contact with the water loop (sensor 9 Table 2.1). An analytical one-dimensional heat transfer equation was used for temperature calculation:

$$T_{surf} = T_{out,w} - \frac{U \cdot (T_{out,w} - T_{Tip,b})}{h_{in,w}} \tag{7}$$

where T is the temperature and the subscripts $surf$, w and b stand for surface, water and brine respectively. The $T_{Tip,b}$ is the average brine temperature of both sensors at the tip of the tube (sensor 2 and 3, see table 2.1), $T_{out,w}$ is the temperature of the sensor close to the outlet of the water (sensor 8, see table 2.1), U is the heat transfer coefficient of water and tube-wall and $h_{in,w}$ is the heat transfer coefficient within the water that is calculated as follows:

$$h_{in,w} = \frac{Nu \cdot \lambda_w}{d_{out} - d_{in}} \tag{8}$$

with λ_w is the thermal conductivity of water, d_{out} and d_{in} are the outer and inner diameter of the coaxial water pipe respectively. Nu is the Nusselt number which depends on the flow rate. Within the laminar flow regime for Re $<$ 2300, $Nu_{lam} = 3.66$. For higher flow rates (maximum tested: 2000 kg/h) with larger velocities we reach a transitional regime between laminar and turbulent flow before reaching the turbulent regime. The Nusselt number in the turbulent regime was calculated using the Dittus and Boelter equation (Incropera et al., 2006).

$$Nu_{tur} = 0.023 \cdot Re^{3/4} \cdot Pr_b^{0.3} \tag{9}$$

In the transitional regime, the Nusselt number was calculated as linear interpolation between the laminar and the turbulent one. As threshold value to the turbulent regime, a Re value of 10000 was assumed, which was calibrated with the experiments. A short validation of the surface temperature calculation is shown in section 4.2.

3 Experimental results at sample level without water flow

3.1 First experimental campaign of contact angle and icing/melting cycles

At the beginning of the project a survey of potential coatings was carried out. The Advisory Board of the project suggested several samples and after discussions on the specific needs for this project several samples were selected by the manufacturers. Besides those we requested s6 which is a commercial coatings that showed good results in Susoff et al. (2013). Finally 12 coatings were selected as summarized in Table 3.1. These coatings were tested using the contact angle indicator to analyse hydrophobicity and durability after multiple icing/melting cycles.

Table 3.1: Coatings analyzed on the first phase of the project

Sample	Chemical class
s1	Polytetrafluoroethylene (PTFE) black
s2	Fluorinated ethylene propylene (FEP) brown
s3	Polysiloxane
s4	Polysiloxane
s5	Perfluoroalkoxy alkanes (PFA), meltable fluoropolymer
s6	Polydimethyl-siloxane
n1	1-K Polysiloxane-urethane resin sol-gel
n2	1-K Polysiloxane-urethane resin sol-gel
n3	2-K Polysiloxane-urethane resin sol-gel
n4	1-K Polysiloxane-urethane resin sol-gel
n5	1-K Polysiloxane-urethane resin sol-gel
n6	1-K Polysiloxane-urethane resin sol-gel

All samples were immersed in a bath of water, iced and melted 230 times, using a climatic chamber. The methodology has been explained in section 2.3.2 and 2.3.1. The contact angle was measured before and after the cycling. All samples were dried before the CA measurements. Results are shown in Fig 3.1, where three types of coatings groups can be observed. The first one with s1, s2, s5 and s6 with initial contact angles (CA) around 115°, thus clearly hydrophobic. Three coatings, n1, n4 and n5 with an initial CA around 85°, thus hydrophilic. The remaining coatings have an initial CA around 105°, hence hydrophobic.

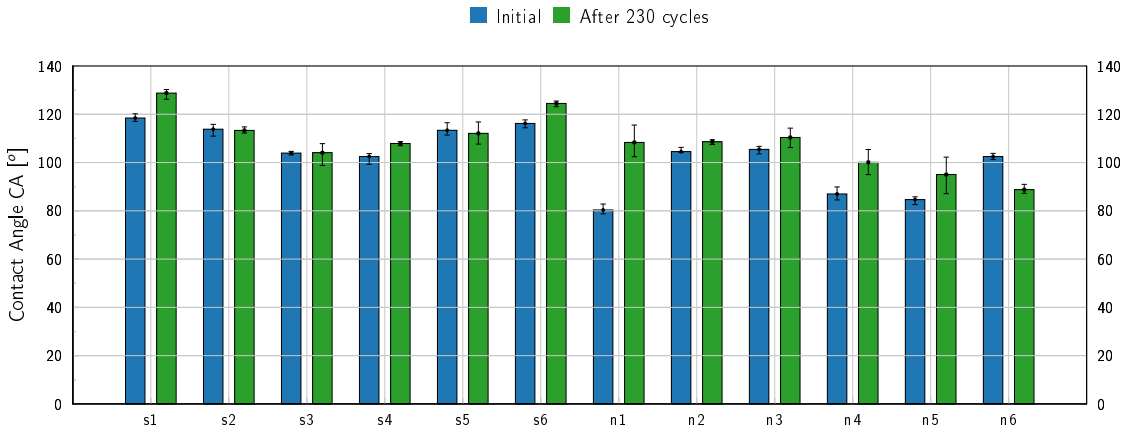

Figure 3.1: Contact angle before and after melting/icing sequences.

It was expected that some of the coatings would become more hydrophilic due to prolonged contact with water. Thus, a degradation of the contact angle after cycles of icing and de-icing was expected. However, only one coating (n6) had a lower CA after the cycles. Some of the coatings, e.g. s1, s6 and n1, n4 and n5 even show a clear increase of the CA, which was not something expected. After the cycling process, all the sample were dried at 100 °C and air could penetrate into micro-cracks. The drying process was made before the CA measurements to avoid any influence of remaining humidity after the prolonged contact with water. Any humidity in the sample will decrease the CA values. Five measurements of the contact angle for each sample in different positions were conducted to assess the surface uniformity and also for uncertainty assessment. The maximum, minimum and averaged CA are presented in Figure 3.1 for each sample before (left) and after (right) of the 230 cycles. It can be observed that the difference between the minimum and maximum CA is larger after the icing/de-icing cycles. This may indicate a change in the uniformity and sample morphology.

The fact that for many coatings an increase of the CA was measured after icing/de-icing made the coatings selection for the next phase difficult. Our aim was to select the coatings that performed the best after icing/de-icing cycles. The fact that a larger scattering in the CA measurements after the aging test was observed for some coatings, could have given a hint of deterioration, but it was not clear enough to take decisions. Therefore, a second experimental campaign was realized with the goal to provide methods which results could help to select the best performing coatings. For that purpose, the CAH and the ice adhesion measurements were used. Also, before doing these experiments, surface morphology was assessed to identify defects like cracks or holes.

3.2 Microscope analyses

The surface morphology was assessed using a simple scanning electron microscope. Defects on coatings can act as nucleation center for icing, thus for icephobic coatings, surfaces without cracks or holes are required. Moreover, for the contact angle measurements, a surface without defects has to be found in order to characterize the material properties, otherwise the contact angle values will be influenced.

Although for some samples the microscope resolution was not sufficient (e.g. for Sample s3), in most of the cases it was enough to observe macroscopic defects. Some of the coatings were not homogeneously applied or holes/cracks have appeared during coating application or during thermal treatment due to solvent evaporation (e.g. for sample s1 and s6).

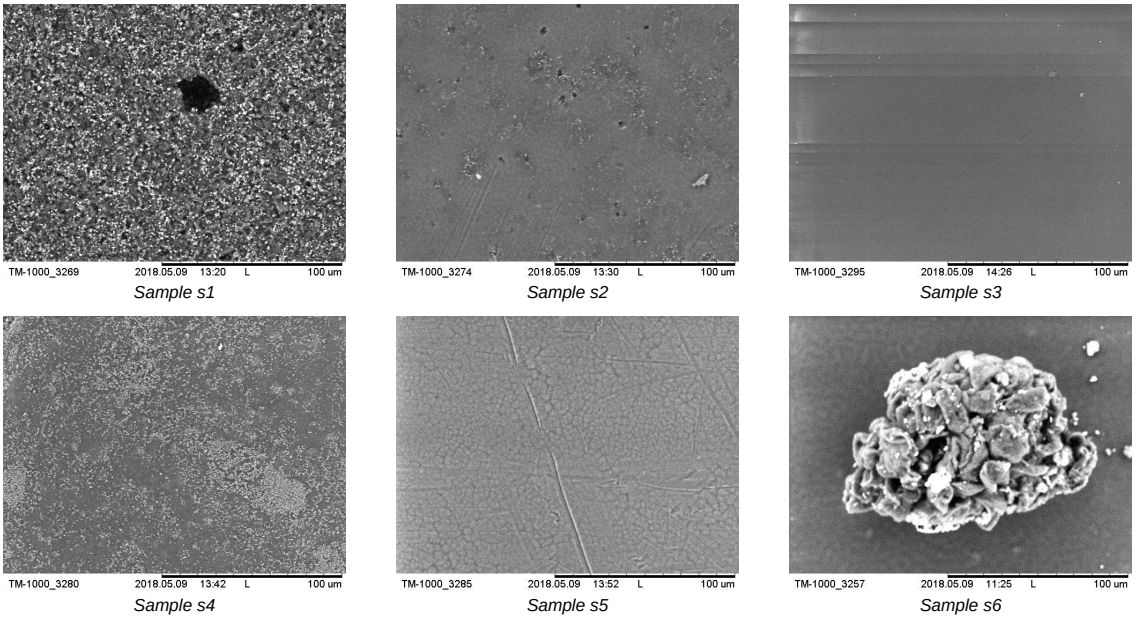

Figure 3.2: Microscope pictures of sample s1, s2, s3, s4, s5 and s6 showing coatings defects like holes and cracks.

3.3 Second experimental campaign

For the second experimental campaign, some coatings that did not show good properties in the first round were dropped. During the course of the project we were in contact with some more companies and research institutes. Within these contacts we detected several new interesting coatings to analyze that could not only be applied to samples but also to tubes if they would show good performance at sample level. Therefore, coatings from m1 to d3 on Table 3.2 were included into the analysis. In total, 13 samples shown in Table 3.2 were measured and characterized.

Table 3.2: Coatings analyzed on the second phase of the project.

Sample	Chemical class
s1	PTFE black
s2	FEP brown
s5	PFA, meltable fluoropolymer
s6	Polydimethyl-siloxane
n2	1-K Polysiloxane-urethane resin sol-gel
n3	2-K Polysiloxane-urethane resin sol-gel
n6	1-K Polysiloxane-urethane resin sol-gel
m1	Fluorochemical modified urethanes
m2	Fluorochemical modified urethanes
m3	Siloxane modified urethanes
m4	Fluorochemical modified urethanes
d1	Hybrid organic/inorganic sol-gel
d2	Silicon rubber

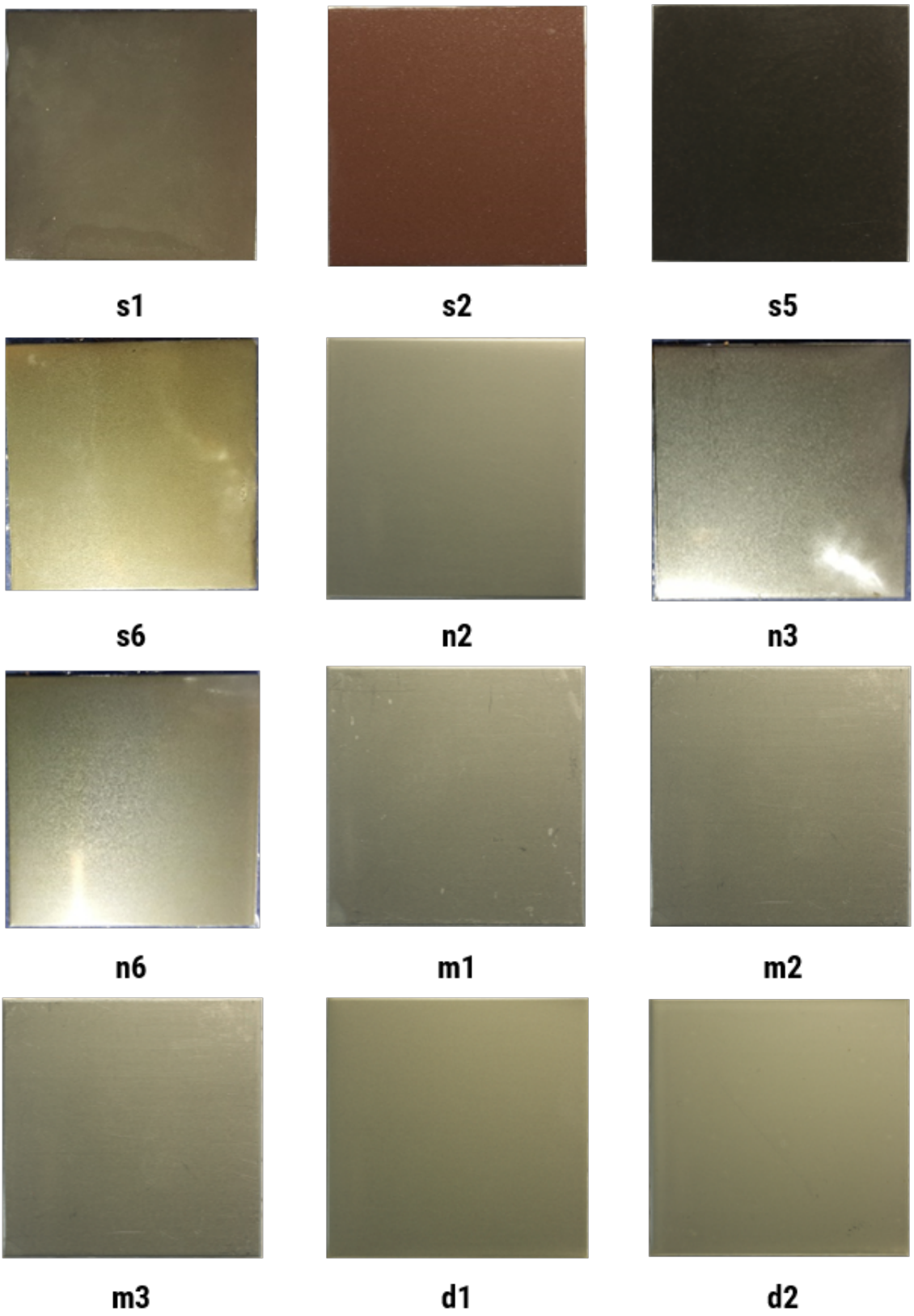

Figure 3.3: Images of selected samples for contact angle hysteresis and ice adhesion measurements (small samples: $50\,\mathrm{mm}^2 \times 50\,\mathrm{mm}^2$).

3.3.1 Contact angle and contact angle hysteresis

The static contact angle is one of the key performance indicators for hydrophobicity. Being hydrophobic does not guarantee icephobicity, but it seems that it is a necessary condition. Results of coatings listed in Table 3.2 are shown in Fig. 3.4. All coatings from Fig. 3.4 show an hydrophobic behaviour with CA$\geq$90°.

The contact angle hysteresis is another key performance indicator for icephobicity. One should notice that there is no standard method to measure the CAH and therefore comparing results from different test methods is difficult. What is clear is that tendencies of measurements using different methods should be the same. For testing the CAH, we have used the methodology described in section 2.3.1. The static, advancing and receding contact angle (CA, CA_{adv}, CA_{rec}) as well as the contact angle hysteresis (CAH) of the coatings described in Table 3.2 are shown in Fig. 3.4.

The coating quality affects considerably the CAH and it was also considered when selecting the coatings for the tube experiments. For example, the sample n3 attracted dust very easily. The coating s6 had many surface defects as can be seen in 3.2. Actually, many samples of the s6 type were coated using a liquid precursor solution. Different companies have tried to apply this coating, but the best method was not found due to project limitations (e.g. budget). This also shows that applying a coating might not be easy task and even a good coating could perform poorly if the deposition method is not optimized. The sample m4 showed lots of scratches on the surface. It was considered that coatings that were not well applied on small scale would cause problems on the tubes were the coated surface would be much larger. Thus, all these coatings, besides the ones with high CAH, were dropped for further experiments. Looking only at the CAH, the best coatings are m2, n2, m1, s2, d1, n3, n6 and d2. All of them have a CAH <9°, which is surprisingly low. The CAH threshold value to consider a coating has good anti-icing properties was <20°.

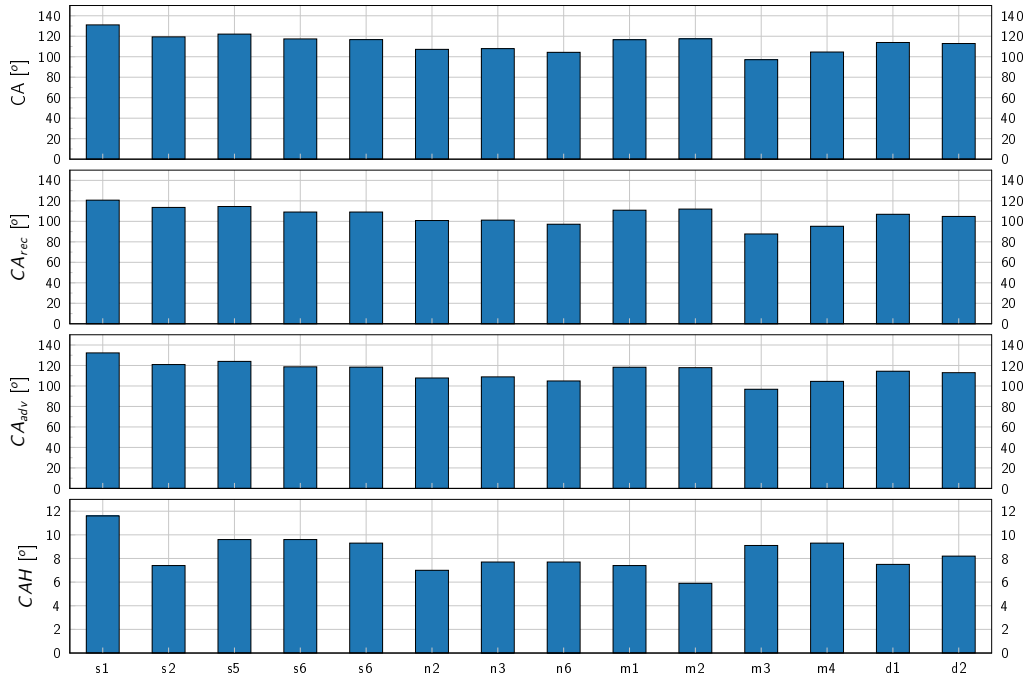

Figure 3.4: Contact angle (CA), receding CA, advancing CA and CA hysteresis (CAH).

3.3.2 Ice adhesion test

Seven coatings were selected for the ice adhesion tests. As explained in section 2.3.3, the ice adhesion test was performed using two methods: a normal stress and a shear stress. The reason to start with the normal stress test was due to the machines available at IWK-HSR. As will be seen below, this test method failed and it was not possible to measure ice adhesion at all, since only cohesive cracks on the ice were observed. Thus, a shear stress method was used afterwards successfully.

Normal stress test: In total, 30 tests were done with only one valid result: a measurement of the d2 coating with a measurement of 140 kPa normal stress. In all other cases, the ice had partially or fully cohesive ruptures (Fig. 3.6). A surprisingly large scattering of the measured force needed to cause cohesive cracks in the ice was observed, with up to a factor of 17 between measurements. The measured forces when the ice broke with cohesive ruptures are shown for four measurement campaigns in Fig. 3.5. The results indicate that not even the cohesive force measurement could be reproduced.

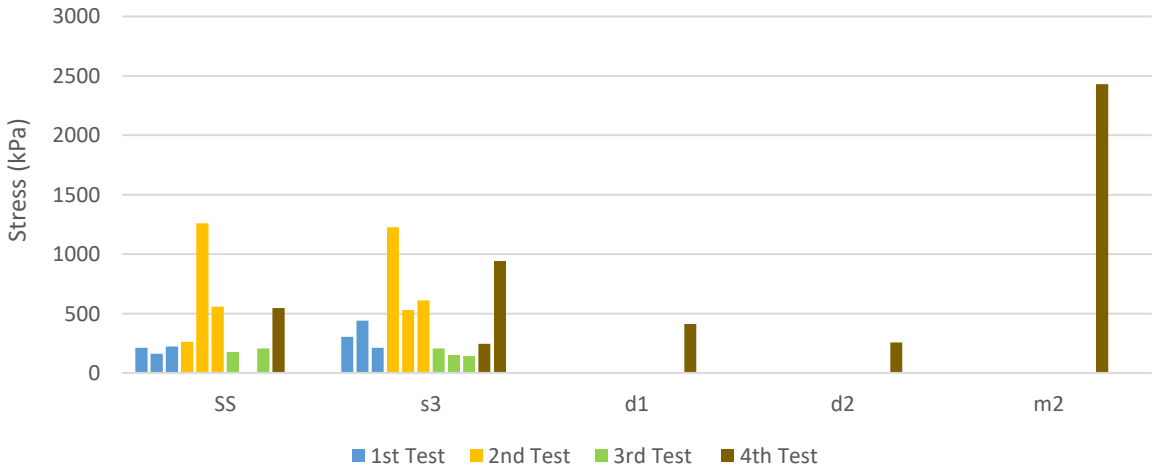

Figure 3.5: Results of the first ice adhesion test with predominantly cohesive ruptures of the ice instead of adhesive detachment. Here only tests with cohesive ruptures are shown.

Figure 3.6: Ice adhesion test with force perpendicular to the sample surface: cohesive ruptures in the ice lead showing remaining ice on both sides: coating (left) and upper sample holder (right).

The failure of the normal stress test determined us to try a second approach, i.e. the shear stress method. The

shear stress method needed more effort for its development, therefore it was not the first choice. However, the ice detachment in a shear stress experiment is more similar to our application case where ice could be potentially removed by a water flow on a heat exchanger. Thus, this might give more insights on the coatings behaviour for supercooling applications.

Share stress test: Results using the shear stress test are shown in Fig. 3.7. On the upper part, the ice adhesion is presented for all coatings from Table 3.2. Three measurements were made for all coatings and two for the SS. The preparation and measurments were done in the same way. All coatings have an ice adhesion much lower than SS. Among all coatings, d2 has shown the best results, with an average ice adhesion of 30kPa.

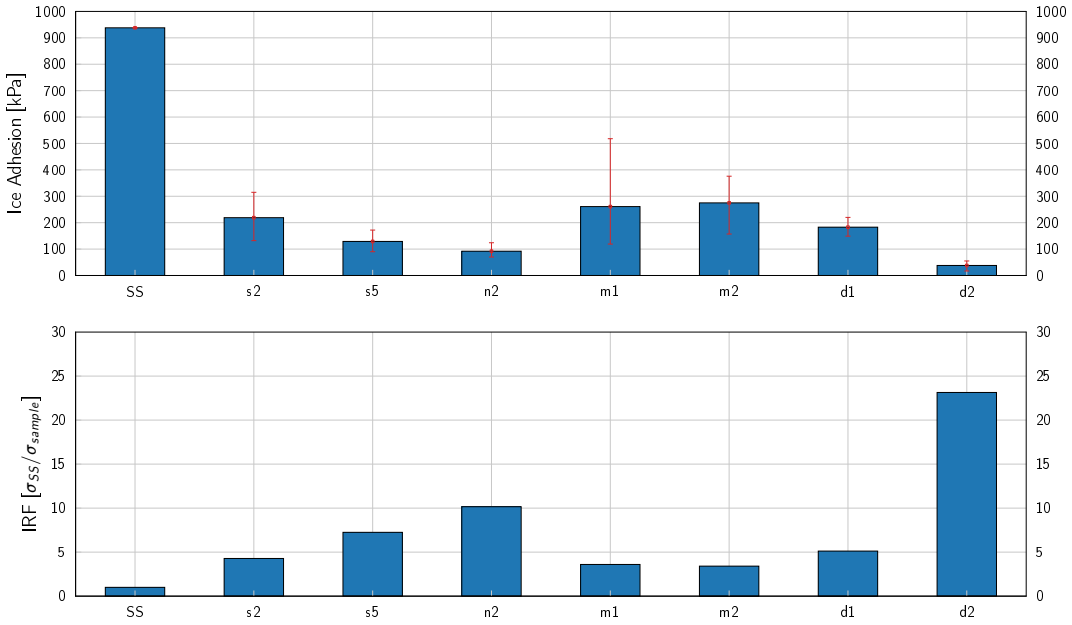

Figure 3.7: Ice adhesion strength using a share stress test and Ice Reduction Factor (IRF) using SS as reference.

On the bottom graph of Fig. 3.7 the Ice Reduction Factor (IRF) respect to the SS ice adhesion is shown. The best values are registered for sample d2 and n2.

Meuler et al. (2010) showed that ice adhesion had a linear relationship with the CA_{rec}[1], i.e. with the surface energy. Nosonovsky and Hejazi (2012) observed that although ice adhesion correlated with CA_{rec}, the size of the micro-cracks at the sold-ice interface could be a major player in the ice-adhesion. Other researchers have not observed a clear relationship with the CA_{rec}, but instead with the CAH (Janjua et al., 2017, Kulinich and Farzaneh, 2009). Recently, Chen et al. (2017) showed that the relation between ice adhesion and CA_{rec} was only observed for hard coatings. Soft coatings such as silicon rubber have lower ice adhesion compared to hard coatings having similar CA_{rec}. The same applies to amiphilic coatings. It is believed that a quasi liquid layer is formed at the coating reducing the ice adhesion significantly (Chen et al., 2017). Therefore, some tendencies observed in the previous research could only apply to some coatings that share the same mechanism for ice-adhesion reduction. In our experiments we could not observe any clear relationship between ice adhesion and CA_{rec} or CAH.

[1]Specifically with $1+\cos(CA_{rec})$

3.4 Selection of coatings for the tube experiments

After the first phase of testing at sample level, seven coatings remained on the potential list for tube experiments: d2, n2, s5, d1, s2, m2 and m1. Due to resource limitations and difficulties in applying the coatings on tubes, it was decided that only four coatings would be used for the tube experiments. Discussing with the manufacturers of the coatings, it was found that coating tubes of the needed size would be a problem for some of the manufacturers. Thus, we had to select those which could actually be applied on tubes. With these constrains, n2, s5 and s2 were disregarded and only m1, m2, d1 and d2 were chosen for the tube experiments. From the coatings that were not further investigated, n2 showed promising results in CAH and ice adhesion test. Unfortunately, the company that developed it was not able to apply the coating on such large tubes.

4 Experiments at tube level with forced convection

As explained in section 3.3.1, four coatings (m2, m1, d1, d2) were selected to assess their ability to supercool water in immersed forced convection conditions. As reference, a polished stainless steel (SS) tube was used with a surface roughness (Ra) of 0.2 μm. Four tubes were sent to the coating manufacturers. Two of them were shipped to United States to be coated with m1 and m2. Unfortunately, after coating the tube with m2, it was found out that the curing process was not good enough and the coating application was not successful. The manufacturer decided to coat the second tube with m2. The coating application was not very good either and this provoked durability issues as will be discussed in section 4.4.1. Due to the cost and time necessary to send back and forth tubes of this size to USA, it was decided not to use m1. As a consequence, only three coated tubes and the reference one (Table 4.1) were experimentally evaluated.

Table 4.1: Selection of coatings to be investigated at tube level in immersed conditions with forced convection.

Sample	Chemical class
d1	Hybrid organic/inorganic sol-gel
d2	Silicon rubber
m2	Fluorochemical modified urethanes
SS	Stainless steel (Ref)

Experiments were conducted using four mass flows 400 kg/h, 800 kg/h, 1600 kg/h and 2000 kg/h which correspond to water velocities of 0.09 m/s, 0.18 m/s, 0.35 m/s and 0.44 m/s flowing on a channel width of 7 mm. As an order of magnitude, the water cooling power (considering heat gains) ranges from 390 W to 720 W for the mass flows evaluated.

4.1 Experimental methodology

In the tube experiments, the water is cooled down gradually by decreasing the brine temperature in steps of 0.2 K. In each step, the brine temperature is kept constant for at least two hours to make sure that thermal equilibrium is reached and freezing is not initiated in this step. The temperature of the last stable step is used as an indication for analyzing the ice preventing properties of the coatings. Freezing does not start at the same temperature in different cycles during one experiment as the freezing temperature is underlying statistical effects. The stable ice-free temperature (temperature at the last step before freezing starts) varies up to about 2 K (see Fig. 4.2) within one experiment. Several cooling cycles are performed for each experiment to get a reliable water freezing temperature and guarantee reproducible results.

The tube experiments can be sensitive to changes in the experimental setup. All experimental details, in particular the setup changes, were recorded in a logbook. Moreover, the water quality was monitored in the first part of the project. The system was always filled with de-ionized water (electrical conductivity of 5.5 μ S/cm). The water electrical conductivity was monitored and the values were about 20 μ S/cm (comparison: drinking

water has about 500 μ S/cm. As conductivity values were in the range of the ones corresponding to de-ionized water, the conductivity was not anymore monitored since August 2019.

4.2 Validation of surface temperature calculation

The temperature on the surface of the coated tube cannot be directly measured, as adding a temperature sensor there could act as a nucleation body and initiate freezing. Therefore, the surface temperature was calculated as described in chapter 2.1. For validation, the surface temperature was measured without supercooling, with a surface temperature sensor (Sensor 9, see Figure 2.12) mounted on a stainless steel tube. This was compared to the calculated value. The goal was to calibrate a simple model that is able to predict the surface temperature in real experiments with coated tubes. The comparison between surface temperature calculation and measurements is shown in Fig. 4.1 for flow rates of 400 kg/h, 800 kg/h and 1600 kg/h. From Reynolds-Number calculation the flow is in a laminar regime for mass flows of 400 kg/h and 800 kg/h and in the transition between laminar and turbulent regimes for a mass flow of 1600 kg/h. In case of a laminar flow at 800 kg/h, the calculated surface temperature fits well with the measured surface temperature as well as for a flow in the transitional regime at 1600 kg/h. For a lower mass flow of 400 kg/h, the measured temperature is about 0.5 K lower than the calculated surface temperature. This could be explained by the higher heat gains in the water loop at lower mass flows. Another reason could be the temperature gradient from the water loop and/or not very precise heat transfer calculations.

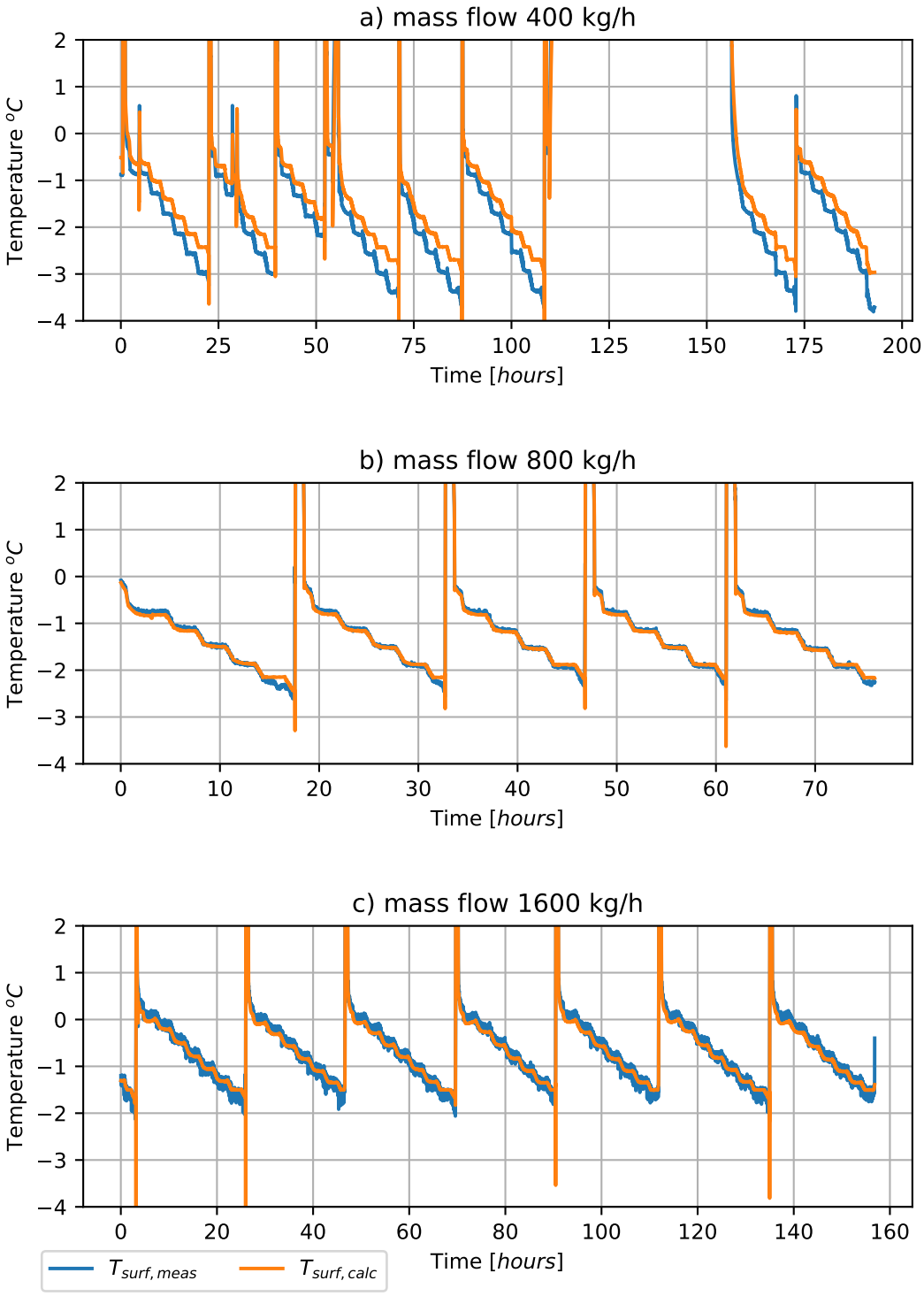

Figure 4.1: Comparison of the surface temperature calculation with experiments for different flow rates.

4.3 Characterization of the coatings by tube experiments

The coatings' ability to depress ice formation was analyzed using the measured brine temperature (sensors 2 and 3 from Fig 2.12) and the calculated water surface temperature before the tip, in water flow direction. Thus, in the coldest region of the water cycle. Temperatures reported correspond to the stable cycle, that is, the temperature of the step before freezing. Thus, the stable ice-free temperature is the temperature that was hold during 2 hours without ice nucleation.

A summary of the results are shown in Table 4.2 and plotted in Fig. 4.2. The error bars in Fig. 4.2 indicate the scattering of measured values for the last stable ice-free temperature. For each experiment, seven cooling cycles have been performed to get more reliable results for each tube.

The performance improvements of coated surfaces are given as a function of the ice-free stable brine temperature difference, which is calculated as follows:

$$\Delta \mathrm{T}_{\mathrm{ice-free}} = \frac{(\mathrm{T}_{\mathrm{coating}} - 273.15) - (\mathrm{T}_{\mathrm{SS}} - 273.15)}{(\mathrm{T}_{\mathrm{SS}} - 273.15)} \tag{10}$$

where all temperatures represent the ice-free stable brine temperature in Kelvin. The $\Delta T_{\text{ice-free}}$ for low mass flows are shown on Table 4.2 as percentages.

Table 4.2: Summary of ice-free stable brine temperature for the reference SS and coated tubes. Improvements of ice-free temperatures difference ($\Delta T_{\text{ice-free}}$) of coatings respect to the SS as shown as percentages in the last two rows.

Mass flow	**SS**	**d1**	**d2**	**m2**
kg/h	°C	°C	°C	°C
400	-5.3	-6.9	-6.6	-7.4
800	-5.5	-7.2	-6.9	-7.8
1600	-	-8.7	-8.0	-
2000	-	-8.9	-7.8	-
$\Delta T_{\text{ice-free}}$ (improvements respect SS)				
400	-	29%	25%	40%
800	-	31%	25%	41%

Comparing the stable ice-free brine temperatures for low mass flow, improvements in the range of 25 % to 41 % due to the use of coatings can be observed. For example, for the mass flow of 800 kg/h, the reference polished stainless steel (SS) tube without coating leads to the highest temperatures, with an average temperature of $-5.5\,°C$. The brine temperature is $-7.2\,°C$ for the tube coated with d1, which is 29 % lower compared to the SS. The lowest brine temperature is reached with the coating m2, with an average of $-7.8\,°C$. This is 41 % lower than in case of the SS tube. No tests were made with the coating m2 at higher mass flows because the coating was deteriorated at a mass flow of 1600 kg/h. This is further discussed in section 4.4.1. High mass flows for SS were measured at the end of the testing phase with some question marks that we have discussed in section 4.4.2 about uncertainties and thus, they are not included here.

As can be observed in Fig. 4.2 (left) higher mass flows allow lower brine temperatures at the tip. As soon as the flow is not any more laminar (transition to turbulent flow starts between 800 kg/h and 1600 kg/h), the local heat transfer between the tube surface and the bulk water increases. Because of that, the local temperature of the water in the "coldest point" (close to tip) is higher than for low mass flows. Therefore, lower brine temperatures within the tube are necessary to initiate freezing. This can be clearly seen when comparing the results from 800 kg/h and 1600 kg/h.

As the brine temperature needs to be decreased by the chiller with increasing mass flow, this gives no information about the mass flow influence and coating thickness on the freezing temperature of the water. The water temperature measured at the outflow of the water tube for a certain brine temperature is mainly depending on the water mass flow. The initiation of freezing depends on the lowest local temperature within the water. However, for higher mass flows, the higher cooling rate due to the increased local heat transfer, could be an

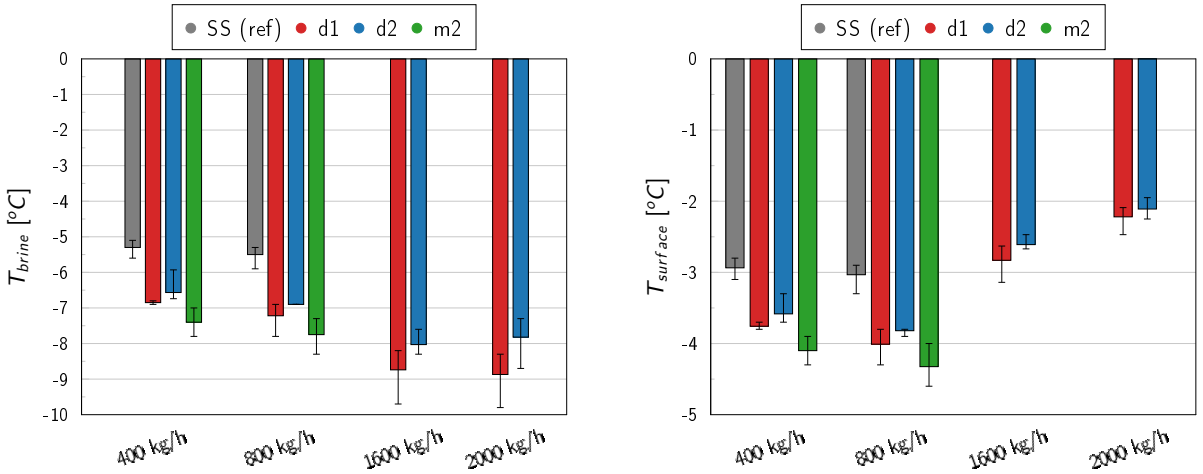

Figure 4.2: Measured brine temperature at the last stable step before freezing (left) and calculated surface temperature (right) at the coldest point of the water side. Results are shown for different mass flows in the water cycle and for the tested coatings s1 (red), d2 (blue), m2 (green). The reference is a not coated, polished stainless steel tube labeled as Inox (grey). The bars indicate the average value a certain mass flow. The error bars indicate the range of temperature measurements.

additional factor for ice initiation. The calculated temperature of the surface between the coated tube and the water flow in the coldest point of the tube ($T_{surface}$) is shown on the right hand side of Fig. 4.2. The comparison of the different coating materials and the reference stainless steel tube gives the same results as for the brine temperature. However, the water temperature reached at stable ice-free conditions is higher at large mass flows in comparison with the T_{brine}, where lower temperatures were observed at high mass flows. As soon as the flow exceeds the threshold of laminar flow regime, the heat transport within the surface and the bulk water rises and the surface layer can't get as cold as in case of laminar flow. Results of $T_{surface}$ seem to indicate that flow velocities might affect the nucleation temperature. Particularly, it seems that that higher velocities provoke nucleation at higher $T_{surface}$. However, more experiments are necessary to discuss if dimensionless numbers such as e.g. Reynolds affect ice nucleation. It should be noted that all coatings analysed are very thin, thus the heat resistance of the coating is not affecting the surface temperature significantly. Therefore, for comparison purposes between coatings for a specific mass flow, T_{brine} can be used, which is a value measured, while $T_{surface}$ needs to be calculated with larger uncertainties.

4.4 Observed problems and open questions

High sensitivity to changes on the experimental setup and uncertainties in measurements are some of the problems we have observed when measuring the coatings under forced flow conditions in the tube experiments. Additionally, coating a tube properly seemed a difficult task. Two tubes coated with m2 by the manufacturer showed coating's defects from the beginning.

4.4.1 Coatings degradation

For the coating d2, the experiment with a mass flow of 800 kg/h was repeated four times within seven weeks. The coated tube was continuously used in this time span. Between 1st and 2nd measurement campaign at 800 kg/h, an experiment with a mass flow of 1600 kg/h was carried out. Between the 3rd and the 4th measurement campaign at 800 kg/h an experiment with a mass flow of 2000 kg/h was conducted. The four measurements are shown on the left part of Fig. 4.3. The brine temperature when no ice was formed is plotted for each measurement campaign. The results indicate a small difference between the three first tests, thus

between week 1 and week 5. However, a 22 % higher temperature for the experiment performed on week 7 can be observed.

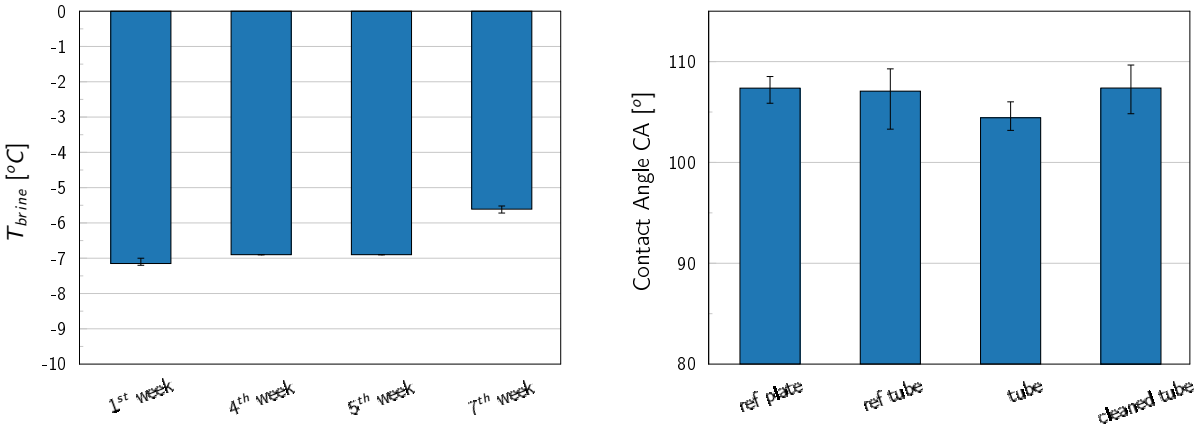

Figure 4.3: Possible effects of degradation or fouling visible in tube measurements with coating d2. Left: Brine temperature for the d2 coating observed in 4 experiments at same mass flow (800 kg/h) over 7 weeks. Right: Contact angle measurements on the tube surface (ref tube: part of the tube without contact to water, tube: tube surface with contact to the water, cleaned tube: tube surface which was in contact to water, but was cleaned afterwards) and on a reference piece - a coated plate (ref plate). The error bars indicate the range of values measured in the different cycles or experiments.

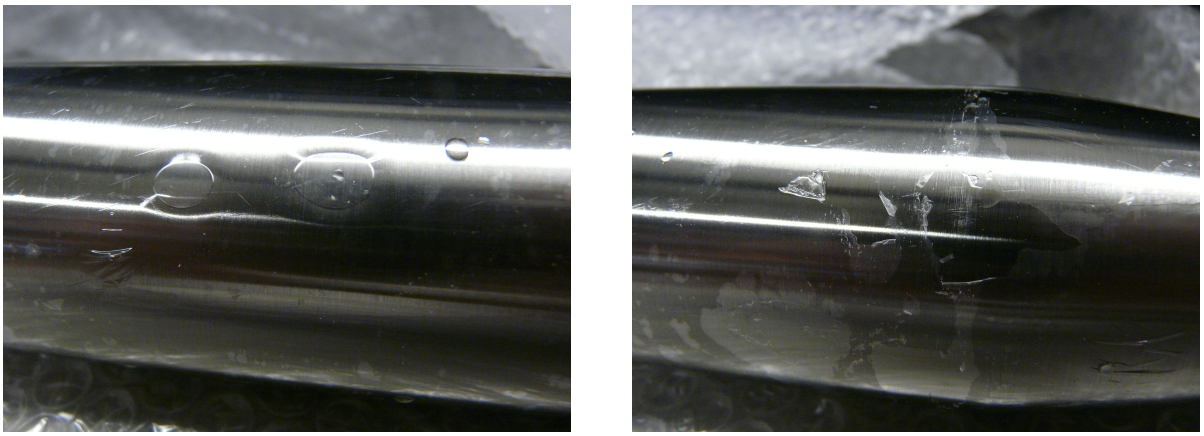

Figure 4.4: Left: Detached coating m2 after running the experiment with a mass flow of 1600 kg/h. Water filled bubbles on the tube surface and right: pilled off coating at the tip oft the tube within the region where the coldest temperatures are reached in the system.

The significant difference in results between week 5 and week 7 could be potentially related either to the coating degradation or to fouling. The results from the last test (week 7) were excluded from the comparison in Fig. 4.2. However, results for d1 and 2000 kg/h might be affected by the same problem and these have been included in Fig. 4.2. In fact, results of T_{brine} for 2000 kg/h should be lower than that of 1600 kg/h, but it is not the case.

A contact angle measurement was performed to check the hydrophobic behaviour of the d2 coating before and after use. Results are shown on the right part of Fig. 4.3. The contact angle was measured for i) a reference flat sample (5 cm x 5 cm) coated with d2 (ref plate), ii) a part of the tube that had no contact with water during the experiment (ref tube), iii) a part of the tube that was exposed to water (tube)

and iv) a part of the tube that was exposed to water, but cleaned afterwards (tube cleaned). The values of the contact angles are the same for the reference flat sample, the reference tube and the cleaned tube. For the uncleaned tube exposed to the water cycle during seven weeks of experiments, the contact angle was lower with 3.0° compared with the reference plate and the value after cleaning the tube. The standard deviation of all contact angle measurements for d2 is 1.7°.Therefore, it is assumed, that the surface properties have changed after being exposed to the water cycle for seven weeks. Further, the coating was inspected chemically by the producer and it showed no defects. Possible explanations would be a microscopic change in the coating that would allow that some water molecules could diffuse inside the coating structure. This would change radically the surface properties. The other explanation might be fouling.

Degradation effects were observed in case of the m2 coating during a flow rate of 1600 kg/h. The defects of the coating were easily observed (Fig. 4.4). At different positions of the tube surface, the water was infiltrated and water bubbles were formed (Fig. 4.4 left hand side). A small initial defect in the coating close to the tip, that seemed not to influence the delay of ice formation in the beginning, increased in size and parts of the coating were pilling off from the tube.

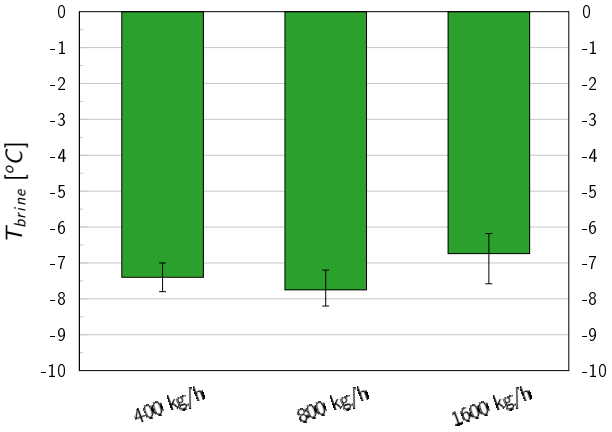

Figure 4.5: Results of the tube experiments with m2 coating including the experiment with a mass flow of 1600 kg/h, where the coating failed during an early stage of the experiment.

The last temperature values recorded in case of stable ice-free conditions for m3 coating in the experiment with a mass flow of 1600 kg/h are shown in Fig. 4.5. The brine temperature in the last step before freezing is expected to be significant lower for a mass flow of 1600 kg/h compared to the lower mass flows. However, this is not observed. The freezing was initiated at higher temperatures when parts of the coating were flowing with the water.

4.4.2 Uncertainties

The outlet temperature of the water was measured at the center of the water-tube (see Fig. 2.12, temperature sensor 8 from the right part of the tube-installation). For low mass flows, this measured outflow temperature might not represent the average value of the water at the outlet because of the radial temperature gradient (the flow is not well mixed in this position). The uncertainty of the measurement for different mass flows cannot be specified. The calculation of the surface temperature was not validated for a flow rate of 2000 kg/h because this experiment is missing for the tube with the surface sensor attached. Effects of the flow behaviour on the surface temperature were only partially considered in the calculation (described in chapter 2.1). As the outlet temperature is fluctuating by about 0.1 °C and it is mainly dependent on the mass flow rate, this temperature is not used for making conclusions directly, but is used for calculating the surface temperature in the coldest point.

As mentioned before in chapter 4.3, the freezing temperature has a stochastic nature and thus even under the same conditions, ice can be formed at different temperatures. To decrease the time needed to for each experimental test, the starting temperature for a new cycle was set individually for each experiment. For evaluating the starting temperature for a new experiment, a new tube or another mass flow, two test-cycles were performed and the brine was cooled down in 0.2 K steps from a temperature that is well above the the freezing temperature for all measured materials. Each step was hold constant for half an hour. From these two

test-cycles, the temperature four steps above the freezing point temperature was used as starting temperature for each cycle in the experiment.

To ensure that the freezing point dependent starting temperature does not hide the stochastic nature of the freezing temperature, a comparison between a fixed starting temperature for each cycle and a variable one is shown in Fig. 4.6. In the uppermost graph, where the initial brine temperature was fixed to −4.4 °C (at the tip) as starting temperature for each cycle, the average brine temperature at the last step before freezing was −8.0 °C. In the lower graph of Fig. 4.6, with an initial brine temperature that is related to the freezing temperature in the test-cycles, the average stable ice-free brine temperature is −8.2 °C.

The experiment with fixed initial brine temperature shows a maximum difference of freezing points of 1.3 K. The experiment with variable starting temperature four steps above the freezing point of the preliminary test case reduces the spread to 0.4 K and thus, it might be that this method influences the stable ice-free temperature that is measured.

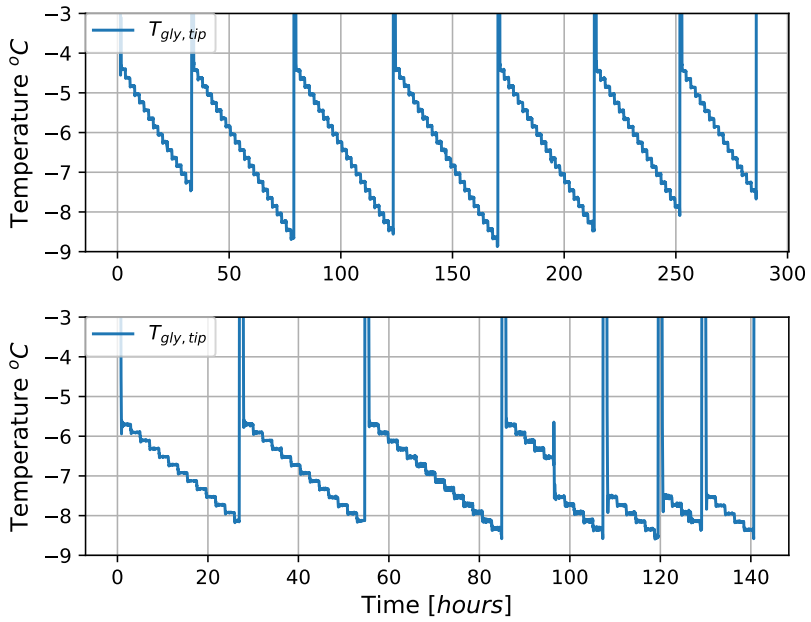

Figure 4.6: Top: Brine temperature at the tip of the tube. Comparison of cycles with fixed starting temperature. Bottom: and with freezing-point dependent starting temperature for the cooling procedure. Experiments with stainless steel tube at a mass flow rate of 1600 kg/h.

.

In the experiments, it was challenging to achieve a complete concentricity between the tubes due to the setup with a long horizontal tube holded only at one part and a coaxial water channel with a width of only 7 mm. A deviation of an angle of 0.3 ° in the fixing point could cause a mismatch of 1 mm at the tip of the tube, which corresponds to 14 % of the channel width. The thickness of the water channel in different positions can not be measured, but can be roughly evaluated visually. Therefore, two people were in charge for every experiment to check the tube position. As 1 mm deviation is already 14 % of the channel thickness, it was not possible to adjust the tube always in the same exact conditions.

Before the experiments with the two highest mass flow rates for the stainless steel tube, the fixation of the bracket that holds the tube was improved. Afterwards, the experiments with the polished stainless steel tube were performed for the mass flow rates of 1600 kg/h and 2000 kg/h since these results were missing. The last stable ice-free brine temperature reached unexpected low values (see Fig 4.7(a)). Therefore, the experiments with lower mass flow (400 kg/h and 800 kg/h) have been repeated as well to check if the results match the first measurements started six months ago. Temperatures were significantly lower than in the first experiments.

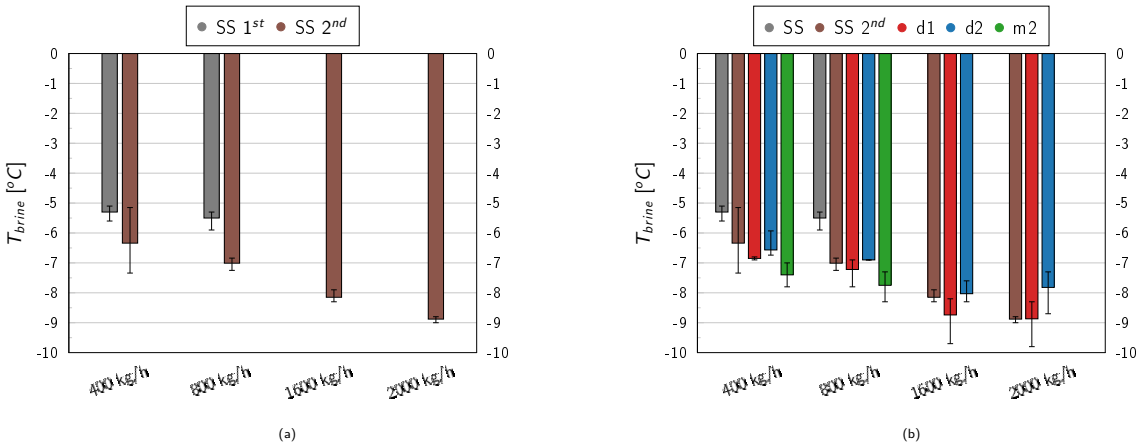

Figure 4.7: (a) First and second round of experiments for the reference stainless steel tubes; (b) All experimental results including those from the first and second campaign for the stainless steel tubes

Results of all experiments including those from the new SS experiments (SS-2nd) are shown in Fig 4.7(b). For low mass flows new results of SS reached almost the values of the tube coated with d2 (the less performing). It is not clear if the concentricity is the only reason for such a difference or if possible air in the system in the first experiments could have affected. It would be necessary to repeat all experiments with an improved setup that would reduce the number of uncertainties. This will be done in the ongoing Horizon 2020 TRI-HP project as discussed in section 6.

4.5 Discussion of the experimental results

The tube experiments for evaluating different coatings under dynamical flow conditions, similar to a heat exchanger, showed significant differences between the coatings. The coating d1 showed the best results in terms of brine and surface temperatures and stable performance with improvements up to 27 % respect to the stainless steel. Coating d2 showed a stable performance as well with better ice inhibiting properties than the reference stainless steel. The m2 coating showed the best results for low mass flows with improvements up to 40 % with respect to stainless steel. However, the coating pilled off in the 3rd experiment with a mass flow of 1600 kg/h. The coating d2 also showed a decrease in performance after 7 weeks of operation. The most likely explanation is due to fouling on the surface.

The values for the lowest stable ice-free outflow temperature of the water are about −0.6 °C for 400 kg/h, −0.3 °C for 800 kg/h, −0.1 °C for 1600 kg/h and 2000 kg/h. A summary of results obtained for the tests performed at atmospheric and immersed conditions for the selected coatings are presented in Table 4.3.

Table 4.3: Summary results for selected coatings analysed in atmospheric conditions.

Sample	**Chemical class**	CA	CAH	Ice adhesion
d1	Hybrid organic/inorganic sol-gel	113.9°	7.5°	183 kPa
d2	Silicon rubber	112.9°	8.2°	33 kPa
m2	Fluorochemical modified urethanes	117.5°	5.9°	275 kPa

An important topic to look at, is the relation between methods used to characterize icephobic coatings for atmospheric conditions and those for underwater, in flow conditions. From the results of Table 4.3 and section 3.3 one can see that CAH and ice adhesion do not correlate and thus they can not be used as the only KPI to characterize icephobic coatings.

Considering the field of use for these coatings, i.e. in supercoolers, it is considered that experiments at tube level

are the most relevant. Thus, the key question is: which measurements from the ones used for characterising icephobic coatings for atmospheric conditions can be used to preselect coatings and avoid expensive and time consuming tube experiments? What seems to be the best indicator is the CAH, since it seems to correlate best with the performance achieved in the tube experiments. Ice adhesion (in the measured range) does not correlate as expected (correlated to CAH). Actually, it seems to have the opposite effect, i.e. the coating with the highest ice adhesion had the best performance in the tube experiment as the lowest surface temperature was achieved in this case. However, this might not be representative due to the low number of cases analysed in the tube experiments. Moreover, we would need to do more ice adhesion experiments to achieve a more reliable average value. A large number of coatings would be necessary to achieve statistically reliable results, which seems difficult using tube experiments since they need a lot of testing time. In summary, this question remains still open.

Different questions have emerged during the tube experiments. There might be an influence of water impurification on the freezing temperatures measured, independent from the measured values of the electrical conductivity in the water. The tube positioning (*"concentricity"*) might have an impact on the measurement results and the starting temperature for each cycle might hide statistical effects if it is set to temperatures that are too close to the freezing point.

A summary of all results including the new experiments from SS are shown in Table 4.4. The improvements of the brine temperature respect to the SS and to the new results of the SS are shown in percentage. It can be observed that the improvements for low mass flows respect to the first SS experiments are very large for all coatings. However, improvements respect to the new SS experiments are lower, although still remarkable for m2, which has between 11 % to 17 % lower ice-free temperature difference ($\Delta T_{\text{ice-free}}$) at low mass flows. Results of m2 for high mass flows are not present since the coating degraded. Results of d1 are between 3 % to 8 % better compared to new SS for mass flows below 2000 kg/h. For the highest mass flow of 2000 kg/h results are very similar. The d2 has better performance at 400 kg/h, very similar at 800 kg/h and 1600 kg/h and clearly worst at 2000 kg/h (which probably was affected by fouling or some kind of degradation). Results of SS at 2000 kg/h are surprisingly good, not only for the low temperature achieved, but also for the low variation between maximum and minimum temperature over seven cycles.

Table 4.4: Summary results including second round of SS experiments with improved experimental setup.

Mass flow	**SS**	**SS-new**	d1	d2	m2
kg/h	°C	°C	°C	°C	°C
400	-5.3	-6.3	-6.9	-6.6	-7.4
800	-5.5	-7.0	-7.2	-6.9	-7.8
1600	-	-8.2	-8.7	-8.0	-
2000	-	-8.9	-8.9	-7.8	-
$\Delta T_{\text{ice-free}}$ (improvements respect SS)					
400	-	20%	29%	25%	40%
800	-	27%	31%	25%	41%
$\Delta T_{\text{ice-free}}$ (improvements respect SS-2$^{\text{nd}}$)					
400	-	-	8%	4%	17%
800	-	-	3%	-2%	11%
1600	-	-	7%	-1%	-
2000	-	-	0%	-12%	-

In summary, these new results of the SS tube leave us with a large uncertainty of the real improvement of the coatings used. It seems to be clear that coatings developed at atmospheric conditions improve the performance, that is, reduce the freezing temperature when immersed in water and submitted to forced convection. However, we have a large uncertainty of by how much. Thus, more experiments are necessary to obtain reliable measurements of improvements.

5 Conclusions

The Slurry-HP II project aimed to find and characterize available icephobic coatings for supercooling applications. In total, 18 coatings were investigated during the project. Two testing procedures were used: the first one involving small coated samples and a second one using coated tubes. In the first case, flat coated samples of 5 cm $\times$ 5 cm were characterized by the methods found in literature for icephobic coatings used in atmospheric conditions. The goal was to select the most promising ones for the tube experiments. The second method was based on testing immersed coated tubes submitted to flow velocities.

At sample level, the most important KPIs used in this project are the contact angle (CA), contact angle hysteresis (CAH) and ice adhesion. At tube level, the ice-free stable temperature at the coldest point of the tube was the main parameter monitored. A relevant KPI at tube level is the supercooling degree. However, it was not feasible to coat tubes long enough to be able to supercool water significantly.

At sample level, different methods were used to select coatings. First, the CA together with a a durability test consisting of icing and melting cycles were used to remove from the coating list those that were not hydrophobic and durable. From the 12 coatings, 4 showed hydrophilic behaviour and were disregarded for future experiments. The rest were and remained hydrophobic after the cycling test, with CA in the range of 105° to 115°. Regarding the durability experiments, only one out of 12 showed significant durability issues and it was disregarded after this test.

A second test was involved to assess the performance of the remaining coatings. For this, the CAH and ice adhesion strength were determined. In this step, 6 promising new coatings were added into the list and were tested together with the 7 selected coatings after the first tests. All these 13 coatings showed CAH below 12°. Therefore, all were good candidates since coatings with CAH $<$25° are considered to have good icephobic properties.

Next, a first ice adhesion test by applying the force at normal direction was performed. This was not successful and most of the experiments failed due to cohesive cracks in ice. Thus, we would not recommend to use a perpendicular (pulling) test for ice adhesion measurements. A second approach was chosen using the shear stress test. Results were found promising: from the seven coatings measured the ice adhesion was between 3 to 23 times lower compared to SS. In particular, two samples showed low ice-adhesion with values below 100 kPa.

From the 13 coatings used in the last phase of small sample experiments, three were used to coat tubes: d1, d2 and m2. Coatings defects, budget restrictions and also the practical possibility to coat a long tube were used as extra criteria to decide which coatings would go to the final tube test.

The tube experiments are more appropriate to simulate the conditions from the final product (a supercooler), where the coating is immersed in flowing water. From the three tested coatings, m2 showed very good freezing depression properties with 40 % higher ice-free temperature difference ($\Delta T_{\text{ice-free}}$) compared to stainless steel. However, the coating degraded after few weeks of testing. A second coating (d1) also showed good anti-freezing properties with 25 % higher $\Delta T_{\text{ice-free}}$ respect to stainless steel. This coating stayed underwater for more than a month and the last results recorded for this sample showed a reduced performance. Possible explanations could be fouling or water molecules diffusing into the coating.

The best coating from the three tested under flow conditions was d1, for which an improvement of $\Delta T_{\text{ice-free}}$ of up to 30 % with respect to the stainless steel tube was achieved. This coating showed to be durable during the whole experiment and it is a good candidate for supercoolers.

A key question we had during this project was if methods to characterize ice-phobic coatings at atmospheric conditions are enough and consistent with the performance of coatings underwater. The answer still remains unclear. Another issue is the lack of standardized methods to assess the performance of icephobic coatings. This makes difficult the comparison of our results with the ones obtained by other research groups.

We consider that the experiments with coated tubes under flow conditions are appropriate to assess icephobic coating used in supercoolers. Moreover, they can be used to establish correlations between some parameters

determined for icephobic coatings used for air applications and for immersed coatings. This would also allow establishing the most relevant methods needed to assess the performance of icephobic coatings for immersed or underwater applications.

After having tested all coatings, several improvements of the experimental setup for the tube test were done. After that, new experiments were conducted for the reference case with a stainless steel tube. Unexpectedly, we observed better results for the reference tube. Experiments using low mass flows were used to compare with previous results. The stable ice-free temperature difference $\Delta T_{\text{ice-free}}$ was decreased by 20 % to 27 % respect to the initial experiments. These changes in performance affect the improvements provided by the coatings. For example the improvement of m2 at a mass flows of 800 kg/h is reduced from 40 % to 17 %. For high mass flows the improvements of d1 are reduced from 30 % to 7 % for 1600 kg/h and not improvements are observed for 2000 kg/h using the d1.This creates high uncertainties in the results of the reference case and future experiments will be conducted to find out the real improvements of coatings respect to the reference of SS.

6 Outlook and next steps

One goal of the current project was to develop a method to characterize icephobic coatings for supercoolers. The idea was to select the promising coatings in a two-step approach: i) at small sample level using the methods recommended for testing icephobic coatings designed for atmospheric conditions and ii) by testing coated tubes to analyse the coatings immersed in water with forced convection. We have realized the second step is very time consuming and its not appropriate to measure the supercooling degree since we would need a way larger heat exchanger surface. The supercooling degree is the most important KPI to measure. From this experience, we believe that a promising approach would be to use the tube set-up to test heat exchangers, but a smaller set-up could be built to test surfaces of few cm^2 with flowing water. We think that similar results could be obtained with this setup compared to the original test tube setup that we have used in this project, simplifying thus the effort needed to characterize a specific coating. Moreover, due to the smaller size of the foreseen setup, it would be easier to obtain the same testing conditions for each coated surface, reducing the uncertainty. It is not only the time needed to test one tube, which for the actual set-up is in the range of one to two weeks per mass flow, but also to construct the tube with soldering pieces and to coat it. Many partners had difficulties in coating such a large tube surface due to ovens' size.

A second difficulty was to avoid ice blockage in the tank when supercooled water was entering the tank. A next step would be to develop an ice releaser that can generate slurries in a continuous way.

The work carried out in Slurry-HP II started an initiative to coordinate a H2020 proposal lead by SPF. This initiative was successful and a H2020 project called TRI-HP [2] is currently running. The overall goal of the TRI-HP project is the development and demonstration of flexible energy-efficient and affordable tri-generation systems to cover heating, cooling and electricity demands. One of the specific targets is to develop and test in the laboratory a solar-ice system using a supercooling ice-slurry heat pump with solar as main heat source. In order to achieve this target, icephobic coatings, supercoolers-evaporators, and propane and CO_2 heat pumps integrating these evaporators will be developed. The set-up developed in Slurry-HP II will be further expanded in TRI-HP and it will be used to test complete heat exchangers.

In the future, we will try to reduce the number of uncertainties of the experimental setup and method with some actions:

- the water will be changed when changing a tube to ensure the same water quality for all tubes.
- fixing of the inner tube will be improved by adding fixing points to ensure a concentric tube position.
- the starting temperature for each cycle within experiments will be set to a constant value for all experiments to consider statistical effects.

[2] www.tri-hp.eu

- the outer tube will be better insulated to avoid heat gains from the room to the water loop.
- the sensor for the water outflow temperature will be replaced in a way that it is positioned in a region of well mixed fluid, where there is no temperature gradient.
- A more precise calculation of the surface temperature based on heat transfer coefficients calibrated using validated CFD simulations.

7 National and international cooperation

A national collaboration was initiated with the Group of the Interfacial Transport Phenomena Laboratory of Thermodynamics in Emerging Technologies in ETH Zürich lead by Professor Poulikakos. Some experiments were conducted in the laboratories of this group by SPF researchers, after some training period. A cooperation was established with the companies ILAG and BUSER.

International cooperation is ongoing with the Institute of Refrigeration, Air-Conditioning, and Environmental Technology (IKKU) from the University of Applied Sciences of Karlsruhe. Professor Michael Kauffeld as expert on ice slurries was part of our advisory board. Collaboration was also initiated with Dr. Thomas Zwieg from Denmark, who developed in 2008 ice repellent coatings for underwater applications using a biomimetical approach. He was also part of the advisory board. We have also started a cooperation with the Danish Institute of Technology (DTI). DTI has sent several samples with two different coatings. Two companies have provided several coatings.

Acknowledgments

The Slurry Hp II project has a long history with many appreciated inputs from several experts in the field. First of all, we would like to tank Professor Michael Kauffeld for the large discussions on the topic of ice slurries and supercooling method. Secondly, to Professor Dimos Poulikakos, Dr. Thomas Shultzius and his group from ETH for allowing us to use their experimental set-up and for the discussions about icephobicity. On this topic we would also like to thank Ricardo Losada from DTI not only for the fruitful discussion about icephobicity, but also to provide coatings to this project. We would also like to thank all companies involved in the provision of coatings and in the application of them. Without coated samples and tubes there would have been no project at all. Last but not least, we would like to thank the Swiss Federal Office of Energy (SFOE) for the financial support received.

References

Carbonell, D., Battaglia, M., Daniel, D. P., and Haller, M. Y. (2017a). *Ice-Ex - Heat Exchanger Analyses for Ice Storages in Solar and Heat Pump Applications*. Institut für Solartechnik SPF for Swiss Federal Office of Energy (SFOE), Research Programme Solar Heat and Heat Storage, CH-3003 Bern.

Carbonell, D., Daniel, D. P., and Haller, M. Y. (2017b). *Slurry-Hp - A feasibility study on the use of a super-cooling ice slurry heat pump for solar heating applications*. Institut für Solartechnik SPF for Swiss Federal Office of Energy (SFOE), Research Programme Heat Pumps and Refrigeration, CH-3003 Bern.

Carbonell, D., Granzotto, M., Battaglia, M., Philippen, D., and Haller, M. Y. (2016a). Experimental investigations of heat exchangers in ice storages for combined solar and heat pump systems. In *11^{th} ISES EuroSun Conference*, Palma (Mallorca), Spain. International Solar Energy Society (ISES).

Carbonell, D., Philippen, D., Battaglia, M., and Haller, M. (2017c). Cost energetic analyses of ice storage heat exchangers in solar-ice systems. In *ISES Soloar World Congress, IEA SHC International Conference on Solar Heating and Cooling for Buildings and Industry*, Abu Dhabi, United Arab Emirates. International Solar Energy Society.

Carbonell, D., Philippen, D., Granzotto, M., and Haller, M. Y. (2016b). Simulation of a solar-ice system for heating applications. system validation with one-year of monitoring data. *Energy and Buildings*, 127(0):846 – 858.

Carbonell, D., Philippen, D., and Haller, M. Y. (2016c). Modeling of an ice storage buried in the ground for solar heating applications. Validations with one year of monitored data from a pilot plant. *Solar Energy*, 125:398–414.

Chen, J., Li, K., Wu, S., Liu, J., Liu, K., and Fan, Q. (2017). Durable Anti-Icing Coatings Based on Self-Sustainable Lubricating Layer. *ACS Omega*, 2(5):2047–2054.

Ensikat, H. J., Schulte, A. J., Koch, K., and Barthlott, W. (2009). Droplets on Superhydrophobic Surfaces: Visualization of the Contact Area by Cryo-Scanning Electron Microscopy. *Langmuir*, 25(22):13077–13083.

Eral, H. B., 't Mannetje, D. J. C. M., and Oh, J. M. (2013). Contact angle hysteresis: a review of fundamentals and applications. *Colloid and Polymer Science*, 291(2):247–260.

Ernst, G. and Kaufeld, M. (2016). Influence of the wall surface roughness on the supercooling degree of water flowing inside a heat exchanger. In *11^{th} Conference on phase change materials and slurries for Refrigeration and air conditioning*, Karlsruhe, Germany. International Journal of Refrigeration (IRR).

Farhadi, S., Farzaneh, M., and Kulinich, S. A. (2011). Anti-icing performance of superhydrophobic surfaces. *Applied Surface Science*, 257(14):6264–6269.

Hejazi, V., Sobolev, K., and Nosonovsky, M. (2013). From superhydrophobicity to icephobicity: forces and interaction analysis. *Nature Scientific Reports*, 3:2194.

Incropera, F. P., Dewitt, D. P., Bergman, T. L., and Lavine, A. S. (2006). *Fundamentals of Heat and Mass Transfer*. John Wiley & Sons, 6^{th} edition.

Janjua, Z. A., Turnbull, B., Choy, K.-L., Pandis, C., Liu, J., Hou, X., and Choi, K.-S. (2017). Performance and durability tests of smart icephobic coatings to reduce ice adhesion. *Applied Surface Science*, 407(Supplement C):555–564.

Jones, P. R., Hao, X., Cruz-Chu, E. R., Rykaczewski, K., Nandy, K., Schutzius, T. M., Varanasi, K. K., Megaridis, C. M., Walther, J. H., and Koumoutsakos, P. (2015). Sustaining dry surfaces under water. *Scientific reports*, 5.

Jung, S., Dorrestijn, M., Raps, D., Das, A., Megaridis, C. M., and Poulikakos, D. (2011). Are Superhydrophobic Surfaces Best for Icephobicity? *Langmuir*, 27(6):3059–3066.

Jung, S., Tiwari, M. K., Doan, N. V., and Poulikakos, D. (2012). Mechanism of supercooled droplet freezing on surfaces. *Nature Communications*, 3:615.

Kim, P., Wong, T.-S., Alvarenga, J., Kreder, M. J., Adorno-Martinez, W. E., and Aizenberg, J. (2012). Liquid-Infused Nanostructured Surfaces with Extreme Anti-Ice and Anti-Frost Performance. *ACS Nano*, 6(8):6569–6577.

Kulinich, S. A., Farhadi, S., Nose, K., and Du, X. W. (2011). Superhydrophobic Surfaces: Are They Really Ice-Repellent? *Langmuir*, 27(1):25–29.

Kulinich, S. A. and Farzaneh, M. (2009). How Wetting Hysteresis Influences Ice Adhesion Strength on Superhydrophobic Surfaces. *Langmuir*, 25(16):8854–8856.

Law, K.-Y. and Zhao, H. (2016). Wetting on flat and smooth surfaces. In Law, K.-Y. and Zhao, H., editors, *Surface Wetting: Characterization, Contact Angle, and Fundamentals*, pages 35–54. Springer International Publishing.

Makkonen, L. (2012). Ice adhesion — theory, measurements and countermeasures. *Journal of Adhesion Science and Technology*, 26:413–445.

Marmur, A. (2006). Underwater Superhydrophobicity:Theoretical Feasibility. *Langmuir*, 22(4):1400–1402.

Meuler, A. J., Smith, J. D., Varanasi, K. K., Mabry, J. M., McKinley, G. H., and Cohen, R. E. (2010). Relationships between water wettability and ice adhesion. *ACS Applied Materials & Interfaces*, 2(11):3100–3110.

Nosonovsky, M. and Hejazi, V. (2012). Why Superhydrophobic Surfaces Are Not Always Icephobic. *ACS Nano*, 6(10):8488–8491.

Philippen, D., Carbonell, D., Haller, M. Y., Frank, E., and Brunold, S. (2014). Auslegung und Betrieb einer hocheffizienten Solarthermie-Wärmepumpen-Heizung mit Eisspeicher. In *24. OTTI Symposium Thermische Solarenergie*, Kloster Banz, Germany.

Philippen, D., Haller, M. Y., Logie, W., Thalmann, M., Brunold, S., and Frank, E. (2012). Development of a heat exchanger that can be de-iced for the use in ice stores in solar thermal heat pump systems. In *Proceedings of EuroSun*, Rijeka and Opatija, Croatia. International Solar Energy Society (ISES).

Rehm, T. (2019). *Eisadhäsionst für metallische Oberflächen*. Masther thesis, HSR, University of Applied Sciences Rapperswil, SPF, Institut for Solar Technology.

Schutzius, T. M., Jung, S., Maitra, T., Eberle, P., Antonini, C., Stamatopoulos, C., and Poulikakos, D. (2015). Physics of Icing and Rational Design of Surfaces with Extraordinary Icephobicity. *Langmuir*, 31(17):4807–4821.

Sojoudi, H., Wang, M., D. Boscher, N., H. McKinley, G., and K. Gleason, K. (2016). Durable and scalable icephobic surfaces: similarities and distinctions from superhydrophobic surfaces. *Soft Matter*, 12(7):1938–1963.

Solomon, B. R., Khalil, K. S., and Varanasi, K. K. (2014). Drag reduction using lubricant-impregnated surfaces in viscous laminar flow. *Langmuir*, 30(36):10970–10976.

Stone, H. A. (2012). Ice-phobic surfaces that are wet. *ACS Nano*, 6(8):6536–6540.

Susoff, M., Siegmann, K., Pfaffenroth, C., and Hirayama, M. (2013). Evaluation of icephobic coatings—Screening of different coatings and influence of roughness. *Applied Surface Science*, 282:870–879.

Upadhyay, V., Galhenage, T., Battocchi, D., and Webster, D. (2017). Amphiphilic icephobic coatings. *Progress in Organic Coatings*, 112:191 – 199.

Wexler, J. S., Grosskopf, A., Chow, M., Fan, Y., Jacobi, I., and Stone, H. A. (2015a). Robust liquid-infused surfaces through patterned wettability. *Soft Matter*, 11:5023–5029.

Wexler, J. S., Jacobi, I., and Stone, H. A. (2015b). Shear-driven failure of liquid-infused surfaces. *Phys. Rev. Lett.*, 114:168301.

Wong, T.-S., Kang, S. H., Tang, S. K. Y., Smythe, E. J., Hatton, B. D., Grinthal, A., and Aizenberg, J. (2011). Bioinspired self-repairing slippery surfaces with pressure-stable omniphobicity. *Nature*, 477:443–447.

Xue, Y., Lv, P., Lin, H., and Duan, H. (2016). Underwater Superhydrophobicity: Stability, Design and Regulation, and Applications. *Applied Mechanics Reviews*, 68(3):030803–030803–38.

Zhang, S., Ouyang, X., Li, J., Gao, S., Han, S., Liu, L., and Wei, H. (2015). Underwater drag-reducing effect of superhydrophobic submarine model. *Langmuir: the ACS journal of surfaces and colloids*, 31(1):587–593.

Zwieg, T. (2005). *Biomimetical ice nucleating coatings*. Phd thesis, Technishen Univerität Dresden, Germany.